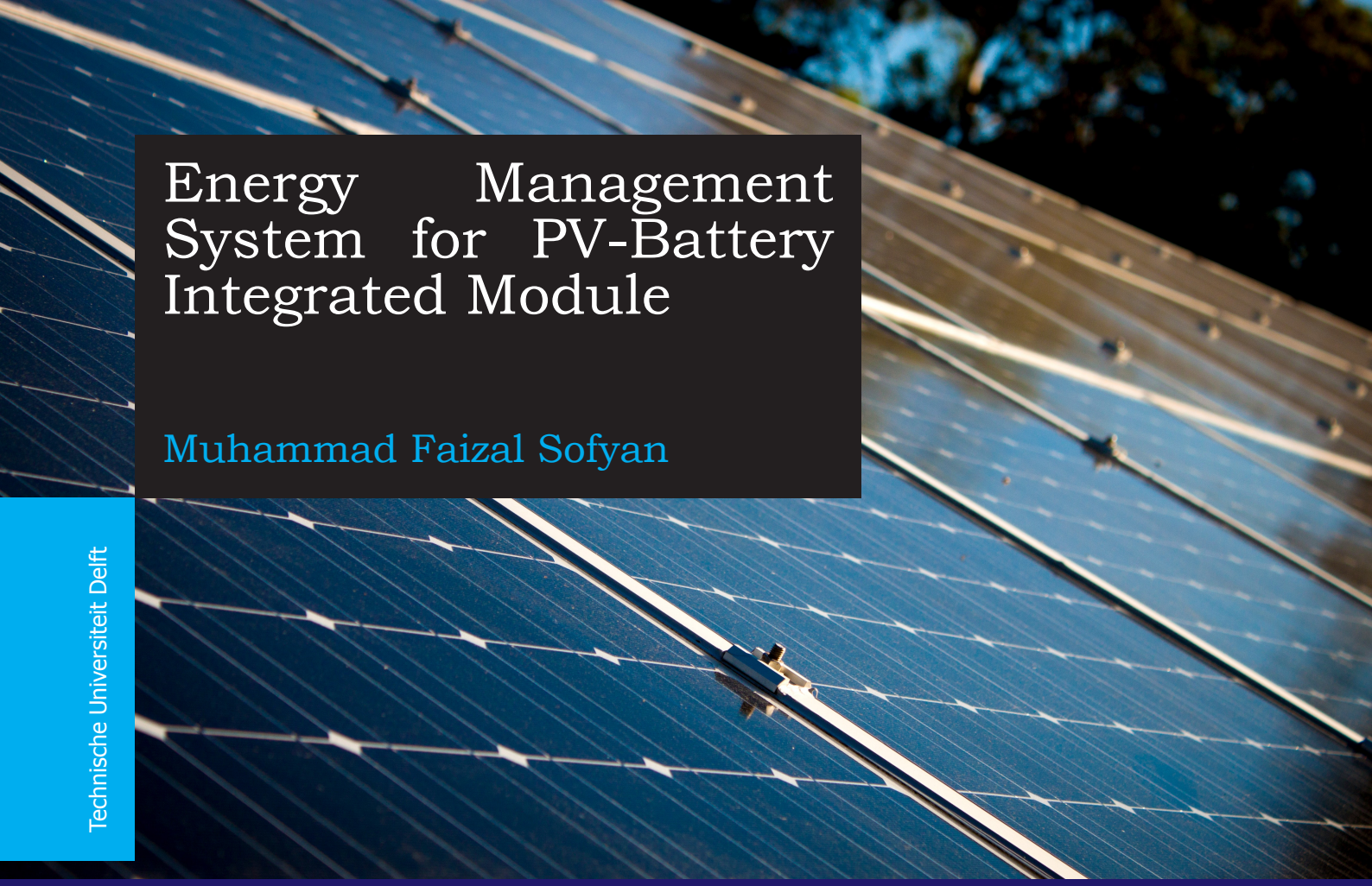

Energy Management System for PV-Battery Integrated Module

Muhammad Faizal Sofyan

Technische Universiteit Delft

TU Delft Delft University of Technology

Challenge the future

Energy Management System for PV-Battery Integrated Module

by

Muhammad Faizal Sofyan

in partial fulfillment of the requirements for the degree of

Master of Science
in Sustainable Energy Technology

at the Delft University of Technology,
to be defended publicly on Thursday, September 27, 2018 at 09:30 AM. .

Supervisor:	Dr.ir. Laura Ramirez Elizondo	DCE&S - TU Delft
Advisor:	Victor Vega Garita M.Sc.	DCE&S - TU Delft
Thesis Committee:	Prof. dr. Pavol Bauer	DCE&S - TU Delft
	Dr.ir. Laura Ramirez Elizondo	DCE&S - TU Delft
	Dr.ir. Jose Rueda Torres	IEPG - TU Delft

An electronic version of this thesis is available at http://repository.tudelft.nl/.

TU Delft Delft University of Technology

Preface

I have been experiencing amazing 2 years in TU Delft thanks to:

1. Allah SWT
2. My parents and my brothers
3. LPDP Scholarship
4. Victor Vega Garita as my Phd supervisor
5. Dr. ir. Laura Ramires Elizondo as my main supervisor
6. Prof. dr. Pavol Bauer and Dr.ir. Jose Rueda Torres as my thesis committee
7. The employees in the DCE&S group
8. PPI Delft
9. SET colleagues
10. Zumba TU Delft

Without them, I would not be able to enjoy the moment in TU Delft.

Muhammad Faizal Sofyan
Delft, September 2018

Abstract

Transition from fossil fuels to renewable sources is desired by both developed and developing countries due to the environmental concern and rapid technological developments. Governments, consumers, and investors have seen the prospect of Photovoltaic (PV) as a prominent technology to fulfill the electricity demand. For the residential-scale PV system,costs of the PV module(s) and the BoS (Balance-of-System) are usually the issue that discourage the consumers from installing PV system in their households. To tackle this issue, the concept of PV-Battery Integrated Module (PBIM) is developed. The operations of the PBIM are similar with typical operations of PV-battery system, which are controlled by the energy management unit. Energy Management System (EMS) is responsible for ensuring the safety of the electrical components and controlling the system operations to make it efficient. Therefore,implementing the suitable EMS is an integral part of establishing the PBIM system.

This research aims to implement a power flow management for the PBIM system to perform two energy management strategies, namely peak shaving and off-grid self-consumption. To achieve that goal, this research focus on selecting the PBIM system architecture, implementing control system and power flow management, and analyzing PBIM system performance on the applications of peak shaving and off-grid self-consumption strategies. Two case studies are introduced in this thesis, namely off-grid PBIM in Cambodia and grid-connected PBIM in the Netherlands.

The chosen system architecture for the PBIM is the DC couple architecture. The PBIM system consists of one PV module, one unidirectional boost converter to perform MPPT and curtail operation, one bidirectional buck-boost converter to handle charging and discharging operation, an inverter to connect the PBIM with an AC load, and a battery bank. There are seven modes of operation in the PBIM system, which are utilized to perform peak shaving and off-grid self-consumption strategies.

For the off-grid PBIM in Cambodia, a 265Wp module and 8 batteries are used. The PV curtail operation is performed mostly during dry season, due to high irradiance. The LLP during rainy season (4%-7%) is much larger than the LLP during dry season (1%-3%), due to big difference in the irradiance between those two seasons. The total LLP for one year operation is 2.6%.

For the grid-connected PBIM in The Netherlands, a 265Wp module and 8 batteries are also used. The peak shaving is performed in this case, hence the battery is being charged during off-peak hours, and the load is supplied by the grid. During peak-hours, the load is supplied by the PV, battery, and the grid. For one PBIM, the system autarky can only a maximum of 16%, hence multiple PBIMs are required to increase the PBIM system autarky for the grid-connected PBIM in the Netherlands.

Contents

List of Figures

List of Tables

Nomenclature

Acronym

AC	Alternating Current
DC	Direct Current
EMS	Energy Management System
LLP	Loss of Load Probability
MATLAB	Matrix Laboratory
MPPT	Maximum Power Point Tracking
PBIM	PV-Battery Integrated Module
PV	Photovoltaic
SOC	State of Charge
STC	Standard Testing Condition

Subscript

batt	Battery
boost	Boost converter
buck-boost	Buck-boost converter
cell	Battery cell
change	Increment
curtail	Curtail
DC	DC bus
fail	Fail
grid	Grid
inv	Inverter
load	Load
M	PV Module
Max	Maximum
mpp	Maximum Power Point
nom	Nominal
peak	Peak
PV	Photovoltaic
ref	Reference

STC Standard Testing Condition

Other Symbols

α Thermal voltage [V]

η_{inv} Efficiency [%]

k_b Boltzmann constant

K_I Temperature coefficient of short-circuit current [%/°C]

K_V Temperature coefficient of open-circuit voltage [%/°C]

n Diode ideality factor [-]

N_S Number of PV cells in series [-]

D Duty cycle [-]

D' Control input converter [-]

G Irradiance [W/m^2]

I_0 Saturation current [A]

I_D Diode current [A]

I_L Light-generated current [A]

I_{SC} Short-circuit voltage [A]

P Power [W]

T Module temperature [°C]

V_{DC} DC bus voltage [V]

V_{OC} Open-circuit voltage [V]

C Capacitance (mF)

I Current (A)

L Inductance (mH)

Q Capacity (Ah)

q Electron charge

R_S Series resistance [Ω]

V Voltage (V)

Controller

e_1 Voltage loop error of boost converter controller

e_2 Current loop error of boost converter controller

e_3 Voltage loop error of buck-boost converter controller

e_4 Current loop error of buck-boost converter controller

$K_{i,i}$ Current integral gain

$K_{i,v}$ Voltage integral gain

$K_{p,i}$ Current proportional gain

$K_{p,v}$ Voltage proportional gain

SW-1 Boost converter switch

SW-2 Buck-boost converter switch (1)

SW-3 Buck-boost converter switch (2)

1

Introduction

1.1. Research Motivation

Transition from fossil fuels to renewable sources is desired by both developed and developing countries due to the environmental concern and rapid technological developments. Governments, consumers, and investors have seen the prospect of Photovoltaic (PV) as a prominent technology to fulfill the electricity demand. This is reflected by the increasing PV system implementations in several scales, such as residential-scale and utility-scale [7]. Figure 1.1 shows that the solar PV generation capacity is constantly growing every year.

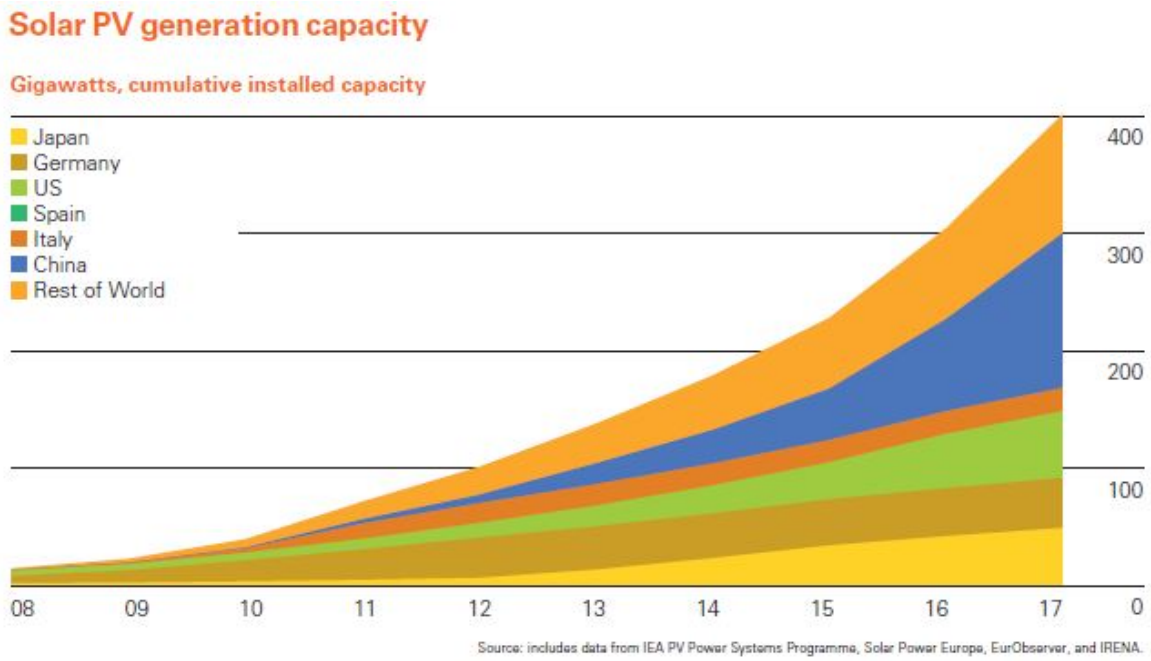

Figure 1.1: Solar PV generation capacity from 2008-2017 [1].

For the residential-scale PV system, costs of the PV module(s) and the BoS (Balance-of-System) are usually the issue that discourage the consumers from installing PV system in their households. To tackle this issue, the concept of PV-Battery Integrated Module (PBIM) is introduced in [8]. PBIM compile the PV module, battery bank, power converters, and power management unit as one package, hence reduce the installation and consultation costs. Since the installation and consultation costs contribute significantly to the overall costs [9], PBIM could become a favourable option to the consumers.

The operations of the PBIM are similar with typical operations of PV-battery system, which are controlled by the energy management unit. Energy Management System (EMS) is responsible for ensuring the safety of the electrical components and controlling the system operations to make it efficient. In a PV-battery system, the EMS is in charge with the PV module operation to make sure that the PV generates power in the most efficient way, and also maintain the State-of-Charge (SOC) of the battery within the operating limits [10]. Therefore, implementing the suitable EMS is an integral part of establishing the PBIM system.

1.2. Research Scope and Objective

The objective of this research is to **'Implement a power flow management for the PBIM system to perform two energy management strategies, namely peak shaving and off-grid self-consumption'**. This research focus on selecting the PBIM system architecture, implementing control system and power flow management, and analyzing PBIM system performance on the applications of peak shaving and off-grid self-consumption strategies.

1.3. Research Questions

1. What is the suitable system architecture for the PBIM system considering the control complexity? (***Ch 2***)
2. How does the control system manage the power flow in the PBIM system to perform peak shaving and off-grid self-consumption strategies? (***Ch 3***)
    - What type of the control mechanisms are used for the DC-DC converters operation, MPPT operation, and PV-curtail operation in the PBIM system?
    - Which modes of operation are needed for the implementation of the chosen energy management strategies?
3. How effective is the off-grid self-consumption strategy for the PBIM application in Cambodia considering the Load of Loss Probability, PV generation reduction, and the energy exchange? (***Ch 5***)
4. How effective is the peak shaving strategy for the PBIM application in the Netherlands considering the system autarky during peak hours? (***Ch 6***)

1.4. Thesis Outline

Chapter 2 - PV-Battery Integrated Module (PBIM)
In this chapter, the concept of PBIM is explained. The selection for the PBIM system architecture is also introduced. Then, the function of each necessary component that build-up the PBIM system is discussed.

Chapter 3 - Energy Management Strategies and Power Flow Management
This chapter introduces two energy management strategies for a PV-Battery system, namely off-grid self-consumption and peak-shaving. Each operation has its own purpose and power flow management. Explanation regarding the power flow modes in the PBIM system and the control mechanism that are used for the DC-DC converters operation, MPPT operation, and PV power reduction are is also provided in this chapter.

Chapter 4 - Modelling the PBIM System
The steady-state models for PV module and battery are given in this chapter. Then, the simulation results of the control operation are presented. In addition, the converters efficiency that are employed for the case studies in the next chapters are presented.

Chapter 5 - Off-Grid PBIM in Cambodia
The dynamic behaviour of an off-grid PBIM system in Cambodia is analyzed in this chapter. Two day simulation is performed for dry and rainy seasons two observe the power flow operation. The annual LLP, PV generation reduction, and the energy fraction of the PBIM system are also discussed.

Chapter 6 - Grid-Connected PBIM in the Netherlands The dynamic operation of a grid-connected PBIM in the Netherlands is analyzed. The performance of multiple PBIMs is also

observed. The annual system autarky and the energy fraction of the PBIM system are also discussed.

Chapter 7 - Conclusions and Recommendations This chapter presents the conclusions of this research and the recommendations for future work.

1.5. Research Contribution

- This research developed an integrated PBIM model, which consists of the PV model, the battery model, and the efficiency curve of the power converters. This model observe the electrical parameters of the PBIM components, such as voltage, current, and power during steady-state condition. These parameters can be used to decide the required sizing of the system and the specification of the power converter (i.e. duty cycle range).
- This research implement a PV-curtail algorithm for the off-grid PBIM application, which manage the power dump of the system. This is one of the improvement for the PBIM research.

2

PV-Battery Integrated Module (PBIM)

To perform a suitable energy management operation for the PBIM system, understanding the concept of the system itself is the first essential step. This chapter provides explanation regarding the PBIM concept. Furthermore, the chosen architecture for the PBIM system and the role of each components are discussed.

2.1. PV-Battery Integration

The idea of integrating a PV with an energy storage has been catching the interest from both researchers and companies. A notion regarding a multifunctional lithium-ion module along with its functional architecture is proposed [2], which resulted a system design that take into account both MPPT and battery charging/discharging control. (Figure 2.1). Next, the concept is developed by introducing an adaptive supervision unit for managing lithium-ion battery [11], and a study about a distributed PV-battery power architecture is conducted [12]. These researches have become the underpin of PV-battery system development.

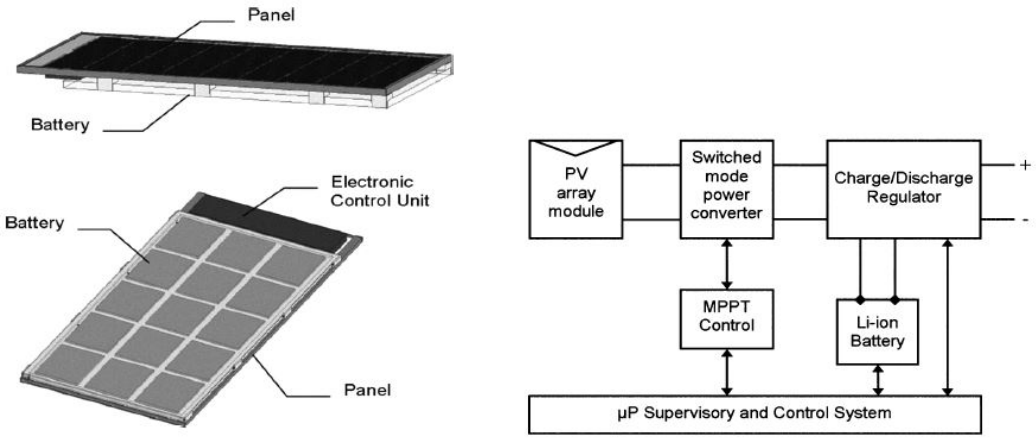

(a) Design. (b) Functional Architecture.

Figure 2.1: The multifunctional lithium-ion module [2].

In [3], a design of PBIM is introduced along with the thermal analysis of the PBIM system (Figure 2.2). This study evaluates the feasibility of PBIM physical integration. Afterwards, a study to determine the proper energy storage sizing for PBIM system is conducted in [13]. This study analyzes the PBIM dynamic behaviour based on the chosen sizing in an off-grid and a grid-connected peak shaving applications. In order to establish the PBIM system implementation, a study about how to manage the power flow in the PBIM system needs to be

conducted. If the power flow management is established, then the suitable energy management strategies can be performed.

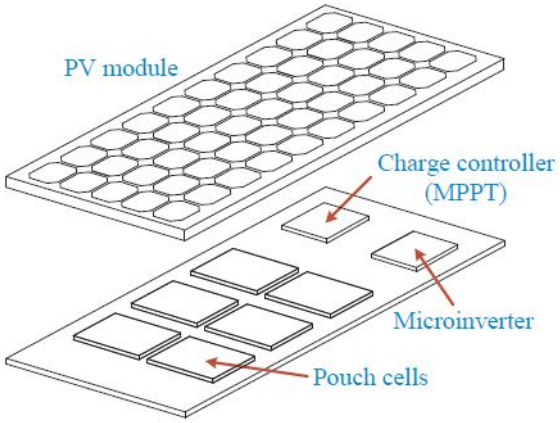

Figure 2.2: PV-Battery Integrated Module concept [3].

2.2. Available System Architecture for PBIM

In this study, the PBIM system focuses on supplying an AC load, which represents a household loads as a whole. There are three types of system architecture for PV-battery system that are commonly used to supply an AC load, namely in-line architecture, DC coupled architecture, and AC coupled architecture. These architectures are different in term of how the PV module, battery, and power electronics are connected altogether. Also, each architecture has its own control system, which can be differentiated by the complexity level. This section will explain how PBIM components are connected and mention what are the required control mechanisms in each architecture.

2.2.1. In-line Architecture

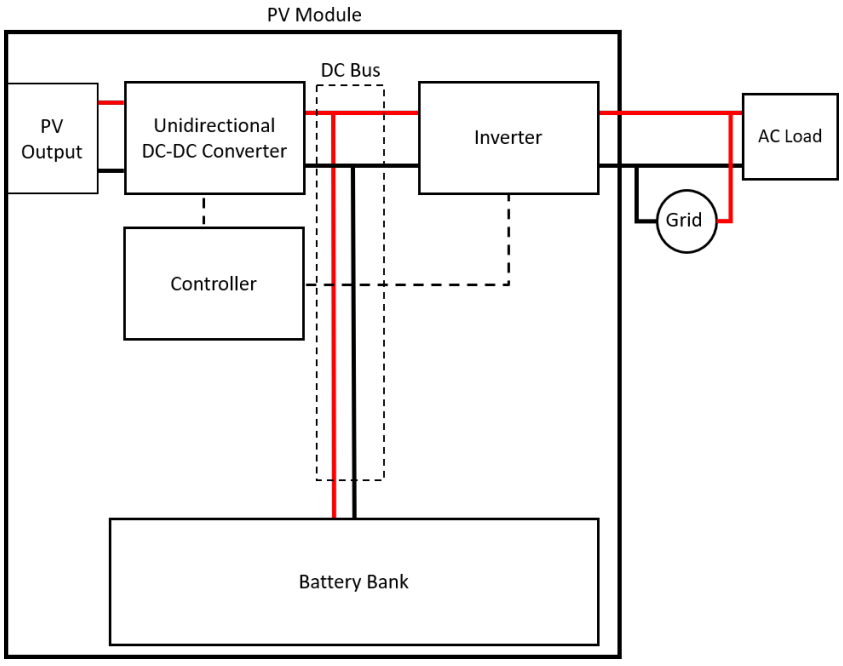

Figure 2.3: In-line architecture.

In this architecture, a DC bus is used as the interconnection between the PV module and the battery. The battery is directly connected to the DC bus, while the PV module is connected to the DC bus using an unidirectional converter. An inverter connects the DC bus with the AC load. The unidirectional DC-DC converter is controlled to perform MPPT task, while the inverter is controlled to perform DC to AC conversion. This architecture limits the flexibility of the battery sizing since the battery voltage must reach the required DC bus voltage. Since the battery voltage dictates the DC bus voltage, the inverter input voltage fluctuates according to the battery parameters. In many cases, the PV module output power is also controlled so that the battery SOC does not exceed the maximum limit. Figure 2.3 shows the in-line architecture for the PBIM. The control system in this architecture consists of the unidirectional DC-DC converter controller, inverter controller, and MPPT algorithm.

2.2.2. DC Coupled Architecture

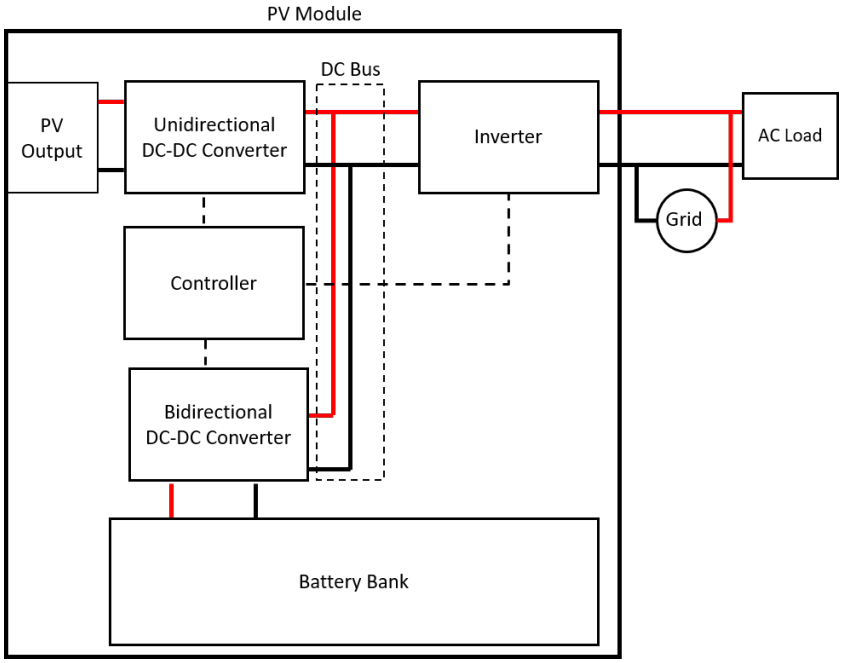

Figure 2.4: DC coupled architecture.

This architecture utilizes a DC bus as the interconnection between the PV module and battery. The PV module is connected to the DC bus using an unidirectional DC-DC converter, while the battery is connected to the DC bus using a bidirectional DC-DC converter. the DC bus is connected to the AC load using an inverter. By utilizing the bidirectional DC-DC converter, the DC bus voltage can be controlled. Since the DC bus voltage can be controlled, the flexibility of battery sizing increases. Since there is only one inverter, the sizing of the inverter is limited to the combination of PV and battery power rating, and this configuration is prone from single point failure since all the power flows through the inverter [14]. The control system in this architecture consists of the unidirectional DC-DC converter controller, bidirectional DC-DC converter controller, inverter controller, and MPPT algorithm. Figure 2.4 shows the DC couple architecture for the PBIM.

2.2.3. AC coupled Architecture

In this architecture, an AC bus is used as the interconnection between the PV module and the battery. An unidirectional power converter is used between the PV module and the AC bus, and a bidirectional power converter is used between the battery and the AC bus. Meanwhile, the grid and the AC load is connected to the AC bus directly. According to the study conducted in [15] and [14], the AC coupled architecture provides flexibility in the

system sizing since the battery bank and the PV module can be sized independently, hence the modularity of the system is accomplished. Figure 2.5 shows the AC coupled architecture for the PBIM. The control system in this architecture consists of The control system in this architecture consists of the unidirectional DC-DC converter controller, bidirectional DC-DC converter controller, inverter controller, and MPPT algorithm. Since there are two inverters, the phase of the inverters output must be synchronized, hence a phase control are required.

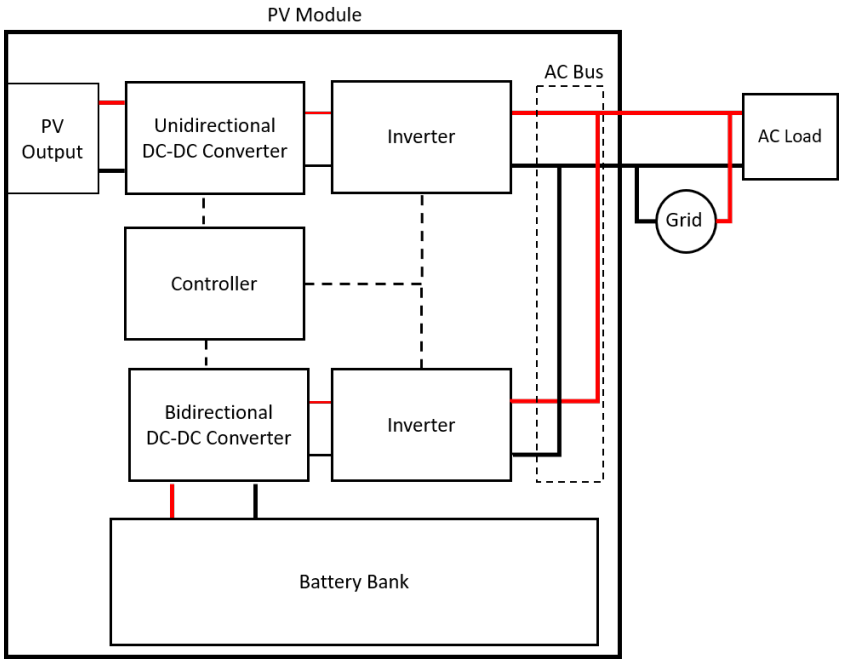

Figure 2.5: AC coupled architecture.

2.3. Components and System Architecture for PBIM

The in-line architecture provide the simplest configuration and minimize the space usage. However, in this architecture, the occurrence of a short circuit in the DC bus will cause serious damage to the battery since the battery is directly connected to the bus [16]. Since the battery is one of the major components in the PBIM system, the battery has to operate safely, hence the in-line architecture will not be used in this study. Both DC couple and Ac couple architectures avoid this battery damage. Next, regarding the control complexity, the DC couple architecture provide simpler control system compared to the AC couple architecture. Also, the power balance in the system can be reflected by the DC bus voltage in the DC couple architecture, hence the control system performance and the power flow operation can be investigated. Therefore, the chosen system architecture for the PBIM in this study is the DC couple architecture.

2.3.1. PV Module

A study regarding the comparison of potential PV module for PBIM is conducted in [15]. Based on the module's weight, rated power, price, and temperature coefficient properties, Jinko Solar Panel JKM265P-60 is chosen as the best alternative for PBIM system. Table 2.1 shows the specification of Jinko Solar Panel.

Parameter	Value
Maximum power ($P_{mpp,STC}$) [W]	265
Maximum power voltage ($V_{mpp,STC}$) [V]	31.4
Maximum power current ($I_{mpp,STC}$) [A]	8.44
Open-circuit voltage ($V_{OC,STC}$) [V]	38.6
Short-circuit current ($I_{SC,STC}$) [A]	9.03
Module length [m]	1.65
Module width [m]	0.99
Number of cells in series (N_S) [-]	60
Temperature coefficient of V_{OC} (K_v) [%/°C]	-0.31
Temperature coefficient of I_{SC} (K_i) [%/°C]	0.06

Table 2.1: Specification of Jinko Solar Panel JKM265P-60 [5].

2.3.2. Energy Storage

The Lithium Ion Prismatic Pouch Cell AMP20M1HD-A from A123 Systems is chosen as the energy storage components in the PBIM system. This battery type is selected due to its compact rectangular form, which is ideal to optimize the space usage [6]. Lithium ion technology is used since it provides good power and energy density [17]. Table 2.1 shows the specification of Lithium ion battery from A123 Systems. The hard-limit of the battery operation is set to be 10% (lower limit) and 90% (upper limit).

Parameter	Value
Cell capacity (Q_{cell}) [Ah]	19.6
Nominal Voltage ($V_{cell,nom}$) [V]	3.3
Voltage at full capacity ($V_{cell,full}$) [V]	3.44
Cell dimensions [mm]	7.25 x 160 x 227

Table 2.2: Specification of Lithium Ion Prismatic Pouch Cell AMP20M1HD-A [6].

2.3.3. System Architecture

To determine the type of converters that are required for in the PBIM system, the DC bus voltage reference has to specified first. The specified DC bus voltage reference in the PBIM system is 48 V. The reason is that this value is higher than the PV open-circuit voltage, and the difference between the DC bus voltage reference and the PV voltage at the maximum power point is justified. If the difference is so large, the duty cycle operation could exceed the maximum duty cycle of the switch in reality. On the other hand, If the difference is so small, the duty cycle operation could be lower than the minimum duty cycle of the switch in the reality. The unidirectional converter has to boost the PV voltage (i.e. 31 V) to reach the DC bus voltage reference (48 V), hence the unidirectional boost converter is used. The bidirectional converter has to boost up the battery voltage during the discharging operation and lower the DC bus voltage during the charging operation, hence the bidirectional buck-boost converter is used. The inverter will have constant modulation since the DC bus voltage is controlled.

2.4. Concluding Remarks

The chosen system architecture for the PBIM is a DC couple architecture. This power electronics in this architecture comprises of an unidirectional boost converter, a bidirectional buck-boost converter, and an inverter.

3

Energy Management Strategies and Power Flow Management

Implementing an energy management strategy on the PBIM system is compulsory to satisfy the consumer demand, and a power flow management is essential to make sure the PBIM performs well and safely. This chapter aims to introduce several energy management strategies that are usually implemented in a PV-battery system. In addition, the power flow modes in the PBIM system are discussed.

3.1. Power Flow Management

A PV-battery system consist of several power stages that adjust the electrical parameters, such as voltage and current, during the operation so that the system can deliver power in the most efficient way and still within the operating limit [18]. In this section, the control system that dictates the operation of each power converter is discussed. Then, the possible power flow modes in the PBIM system are presented.

3.1.1. Control System

Based on the system architecture explained in Section 2.3.3, the unidirectional boost converter, the bidirectional buck-boost converter, and the inverter are the ones who perform power stage operations, so that the several power flow modes can be employed. The control system in the PBIM system consists of four parts, namely MPPT algorithm, PV-curtail algorithm, unidirectional boost converter controller, and bidirectional buck-boost converter controller. The inverter will operate in constant modulation, assuming that the DC bus voltage is always maintained at the reference value, and therefore no controller are required for the inverter, only a constant modulation signal will be sent to the inverter.

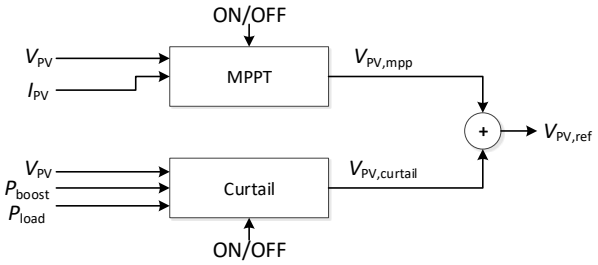

Figure 3.1: Choosing the PV voltage reference.

Figure 3.1 shows how the PV voltage reference obtained. If the MPPT algorithm is off, then the PV-curtail algorithm will provide the PV voltage reference, and vice versa. Equation 3.1 define the PV power (P_{PV}) when the MPPT algorithm is used, while Equation 3.2 define the (P_{PV}) when the PV-curtail algorithm is used. The PV voltage at the maximum power point ($V_{PV,mpp}$), PV current at the maximum power point ($I_{PV,mpp}$), PV voltage during the curtail operation ($V_{PV,curtail}$), and PV current during the curtail operation ($I_{PV,curtail}$) are obtained from the power flow management process.

$$P_{PV} = V_{PV,mpp} \cdot I_{PV,mpp} \tag{3.1}$$

$$P_{PV} = V_{PV,curtail} \cdot I_{PV,curtail} \tag{3.2}$$

MPPT Algorithm

An MPPT algorithm is employed to ensure that the PV operates at its maximum power point. The incremental conductance method is used in this study. Figure 3.2 shows the MPPT algorithm using incremental conductance method. The value of the voltage increment (V_{change}) is chosen to be 0.1 V. The output of this MPPT algorithm, which is the $V_{PV,mpp}$, will be used in the boost converter feedback loop control as the PV voltage reference.

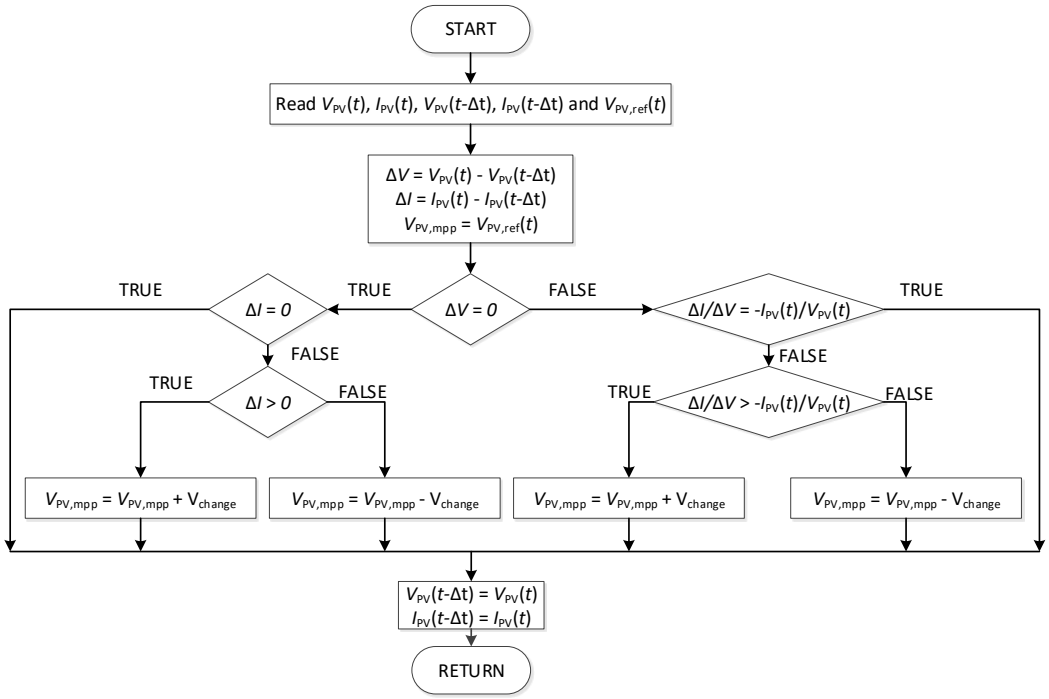

Figure 3.2: MPPT Algorithm.

PV-Curtail Algorithm

One issue that needs to be handle during the operation of an off-grid PV-battery system is regarding how to manage the excess energy from PV generation. If the battery is full, the load is already fulfilled, and there is an excess power from the PV generation, the excess power have to be dumped in order to maintain the system balance (i.e. DC bus voltage). One way to manage this excess energy is to curtail the PV generation when the battery is already full. The PV has to operates far away from the maximum power point to produce power less than the load demand. If the PV generation is less than the load demand, the battery has to be discharged to fulfill the load demand. Hence, the battery will not exceed the upper SOC limit, and no excess power need to be dumped. Figure 3.3 shows the PV-curtail algorithm.

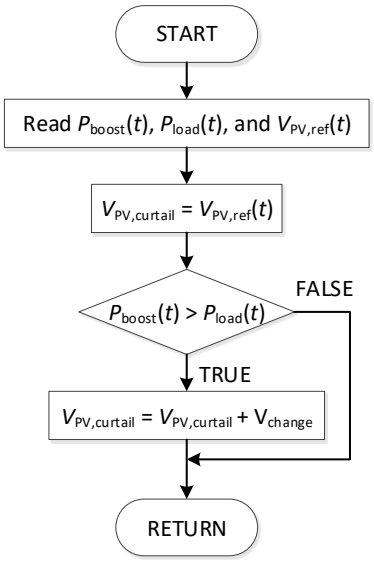

Figure 3.3: PV Curtail Algorithm.

The value of the voltage increment (V_{change}) is chosen to be 0.1 V. At the initial condition, the PV operates at the maximum power point , then the PV voltage reference increasing and move the PV operating point to the right side of the P-V curve, so the PV power is reduced. Even though the right side of the maximum power point is steeper than the left side, the voltage range in the right side is more narrow than in the left side, hence the boost converter does not have to operate with a wide duty cycle range. The output of this algorithm, which is the $V_{PV,curtail}$, will be used in the boost converter feedback loop control as the PV voltage reference.

Unidirectional Boost Converter controller

The unidirectional boost converter operates by adjusting the duty cycle (1-D'_{boost}) of SW-1 (boost converter switch). (1-D'_{boost}) is obtained from the feedback loop control shown in Figure 3.4. Two proportional-integral (PI) controllers are used in this feedback loop control. The inner loop controls the PV current, and the outer loop control the PV voltage. The PV voltage reference from the MPPT/PV-curtail algorithm is used as the reference. The output of this controller is sent to the pulse width modulation (PWM) generator, and SW-1 will operate according to the chosen duty cycle value. Therefore, the desired PV voltage can be achieved.

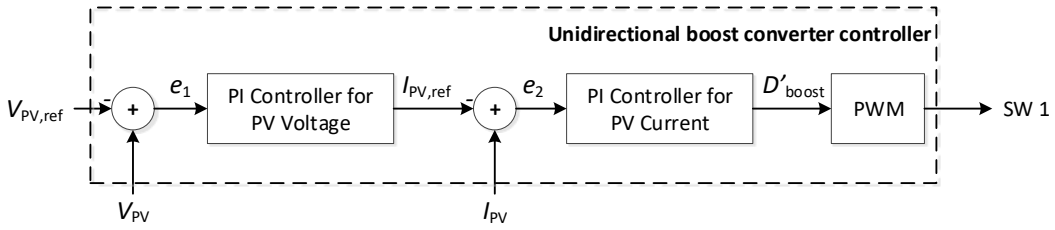

Figure 3.4: Feedback loop for boost converter.

The following equations express the processes of determining the parameters in the feedback loop, where $K_{p,v}$, $K_{i,v}$, $K_{p,i}$, and $K_{i,i}$ are the coefficients of the PI controllers.

$$e_1(t) = V_{\mathrm{PV}}(t - \Delta t) - V_{\mathrm{PV,ref}}(t) \tag{3.3}$$

$$e_2(t) = I_{\mathrm{PV}}(t - \Delta t) - I_{\mathrm{PV,ref}}(t) \tag{3.4}$$

$$I_{\mathrm{PV,ref}}(t) = \mathrm{K_{p,v}} \cdot e_1(t) + \mathrm{K_{i,v}} \cdot \int_0^t e_1(t)dt \tag{3.5}$$

$$D'_{\mathrm{boost}}(t) = \mathrm{K_{p,i}} \cdot e_2(t) + \mathrm{K_{i,i}} \cdot \int_0^t e_2(t)dt \tag{3.6}$$

Bidirectional Buck-Boost Converter Controller

The bidirectional buck-boost converter operates by adjusting the duty cycle of the buck-boost converter switches. SW-2 depends on $D_{\text{buck-boost}}$, while SW-3 depends on (1-$D_{\text{buck-boost}}$), which are obtained from the feedback loop control shown in Figure 3.5. Two proportional-integral (PI) controllers are used in this feedback loop control. The inner loop controls the battery current, and the outer loop control the DC bus voltage. The output of this controller are sent to the pulse width modulation (PWM) generator, and SW-2 and SW-3 will operate according to the chosen duty cycle value. Therefore, the desired DC bu voltage can be achieved.

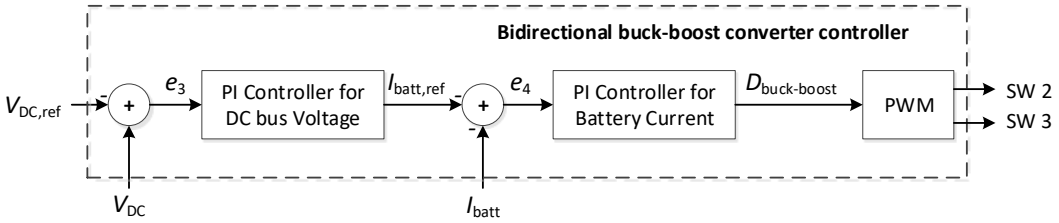

Figure 3.5: Feedback loop for buck-boost converter.

The following equations express the processes of determining the parameters in the feedback loop, where $\mathrm{K_{p,v}}$, $\mathrm{K_{i,v}}$, $\mathrm{K_{p,i}}$, and $\mathrm{K_{i,i}}$ are the coefficients of the PI controllers.

$$e_3(t) = V_{\mathrm{DC}}(t - 1) - V_{\mathrm{DC,ref}}(t) \tag{3.7}$$

$$e_4(t) = I_{\mathrm{batt}}(t - 1) - I_{\mathrm{batt,ref}}(t) \tag{3.8}$$

$$I_{\mathrm{batt,ref}}(t) = \mathrm{K_{p,v}} \cdot e_3(t) + \mathrm{K_{i,v}} \cdot \int_0^t e_3(t)dt \tag{3.9}$$

$$D_{\text{buck-boost}}(t) = \mathrm{K_{p,i}} \cdot e_4(t) + \mathrm{K_{i,i}} \cdot \int_0^t e_4(t)dt \tag{3.10}$$

3.1.2. Modes of Operation

The possible power flow modes in the PBIM system using DC coupled architecture are presented in Figure 3.6, and the operation of each converter during each mode is summarized in Table 3.1

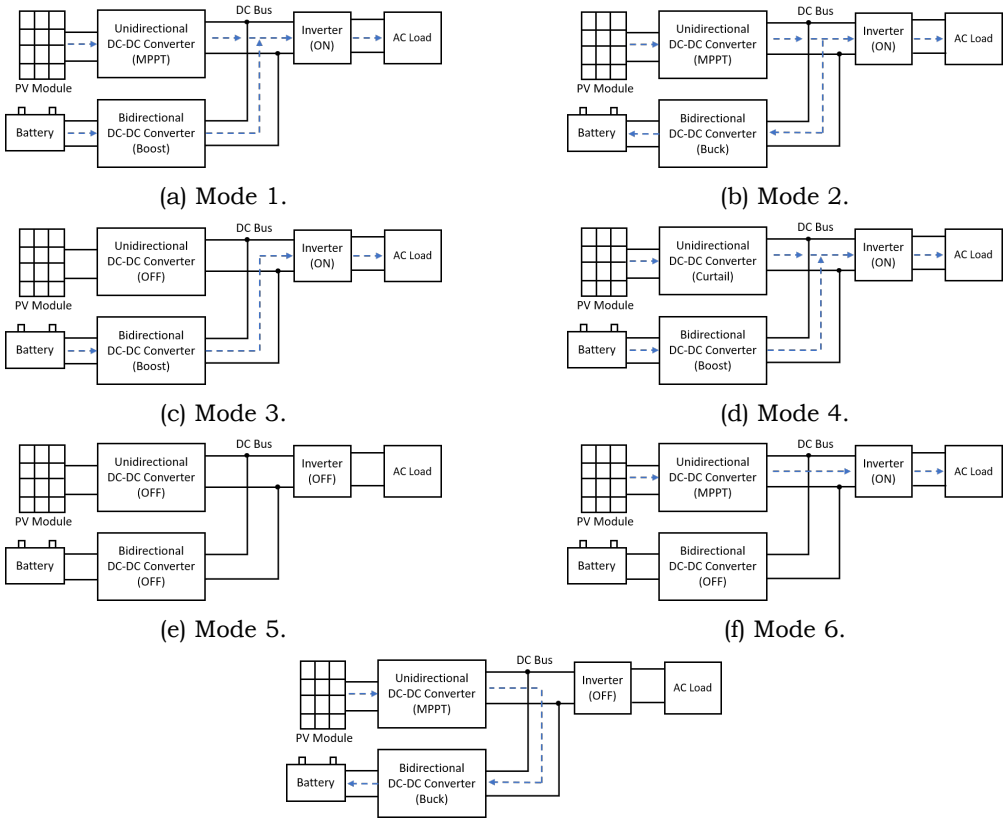

(a) Mode 1. (b) Mode 2.

(c) Mode 3. (d) Mode 4.

(e) Mode 5. (f) Mode 6.

(g) Mode 7.

Figure 3.6: Power flow modes in the PBIM system.

- **Mode 1**: PV is connected, the unidirectional converter performs MPPT operation, the battery is discharging, bidirectional converter performs boost operation, inverter is on, and the load is connected. Employed in the off-grid and peak shaving applications.

- **Mode 2**: PV is connected, the unidirectional converter performs MPPT operation, the battery is charging, bidirectional converter performs buck operation, inverter is on, and the load is connected. Employed in the off-grid application.

- **Mode 3**: PV is disconnected. The unidirectional converter switches off, the battery is discharging, bidirectional converter performs boost operation, inverter is on, and the load is connected. Employed in the off-grid and peak shaving applications.

- **Mode 4**: PV is connected, the unidirectional converter performs curtail operation, the battery is discharging, bidirectional converter performs boost operation, inverter is on, and the load is connected. Employed in the off-grid application.

- **Mode 5**: PV is disconnected, battery is disconnected, and all the converter switch off. The load is disconnected. Occurs in the off-grid and peak shaving applications.

- **Mode 6**: PV is connected, the unidirectional converter performs MPPT operation, battery is disconnected, inverter switchs on, and the load is connected. Employed in the peak shaving application.

- **Mode 7**: PV is connected, the unidirectional converter performs MPPT operation, bidirectional converter performs buck operation, battery is charging, inverter switchs off, and the load is disconnected.

Converter	Mode 1	Mode 2	Mode 3	Mode 4	Mode 5	Mode 6	Mode 7
Unidirectional	MPPT	MPPT	OFF	Curtail	OFF	MPPT	MPPT
Bidirectional	Boost	Buck	Boost	Boost	OFF	OFF	Buck
Inverter	ON	ON	ON	ON	OFF	ON	OFF

Table 3.1: Converter operation for various power flow modes.

3.2. Energy Management Strategies for a PV-Battery System

Energy management strategy is defined as structured procedures to manage the energy quantity and lessen the energy cost according to the consumer requirements [19]. The selection of the suitable energy management strategies are based on the type of energy system and its components. For a PV-battery system, the following strategies can be performed, namely off-grid self-consumption and peak shaving.

3.2.1. Off-Grid Self-Consumption

Due to the intermittent energy production from the PV, self-consumption method utilizes the battery in order to make sure the load is always met in an off-grid PV-battery system [20] (Figure 3.7). If the load is already met and there is an energy surplus from the PV production, the energy surplus is stored in the battery as long as the battery is not fully charged. Meanwhile, if the PV production cannot keep up the load demand, the battery will cover the deficit power as long as the battery is not fully discharged. However, some fails will occur when the PV-battery system cannot meet the load demand. On the other hand, the excess energy from the PV need to be dumped when the battery is full. In the latter situation, a PV-curtail operation will be performed. Figure 3.8 presents the off-grid self-consumption algorithm.

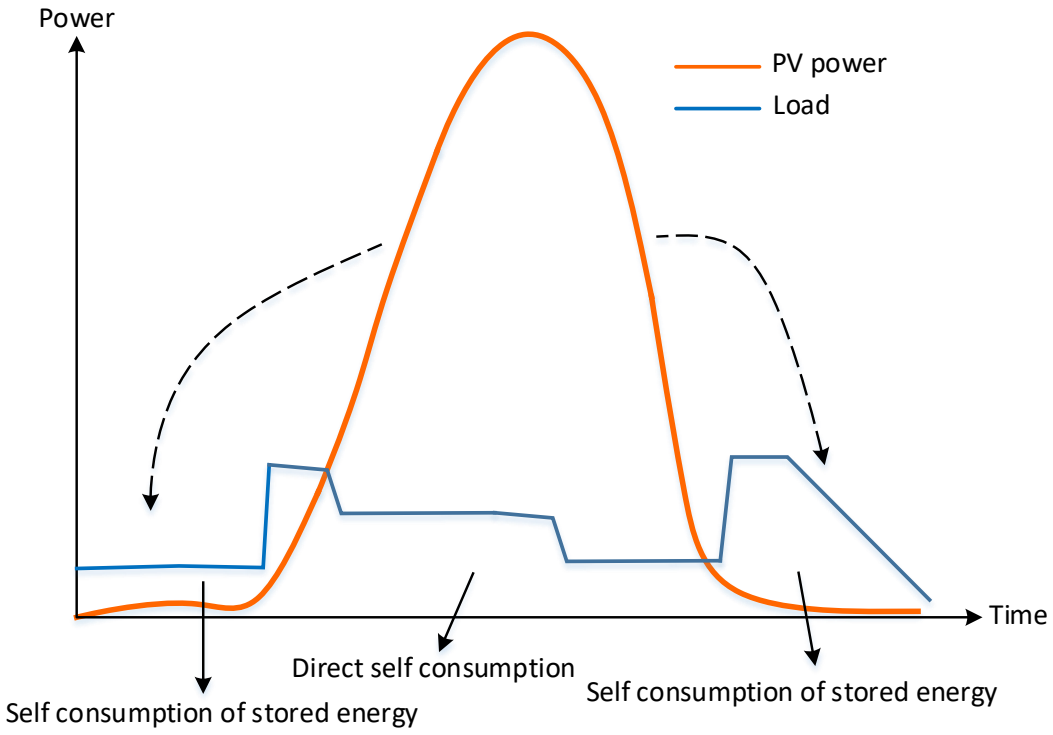

Figure 3.7: Off-grid self-consumption principle.

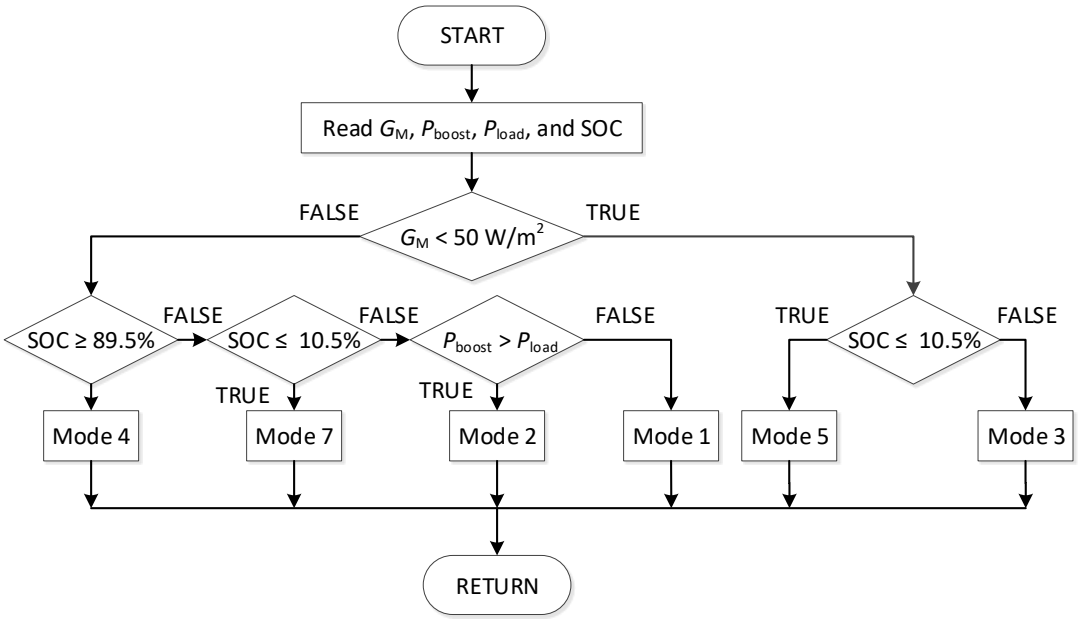

Figure 3.8: Off-grid self-consumption algorithm.

In the off-grid self-consumption algorithm, the values of irradiance, unidirectional boost converter output power, load demand, and the battery SOC are measured to determine which mode is going to operate. The minimum irradiance required to utilize the PV module is set to be 50 W/m^2. The operating limit of the battery is set to be 10.5% (lower limit) and 89.5% (upper limit). There are six modes employed in the off-grid self-consumption strategy.

- **Mode 1:** This mode occurs when there is not enough power from the PV side to supply the load demand, and the battery SOC still within the operating limit. The battery will be used to supply the remaining load, and the PV generates at the maximum power point. The power balance in this mode is stated in Equation 3.11.

$$P_{\text{boost}} \cdot \eta_{\text{inv}} + P_{\text{batt}}^{\text{out}} \cdot \eta_{\text{buck-boost}} \cdot \eta_{\text{inv}} - P_{\text{load}} = 0 \tag{3.11}$$

- **Mode 2:** This mode occurs when there is power surplus from the PV sides, and the battery SOC still within the operating limit. The power surplus will be used to charge the battery. The power balance in this mode is stated in Equation 3.12.

$$P_{\text{boost}} - \frac{P_{\text{load}}}{\eta_{\text{inv}}} - \frac{P_{\text{batt}}^{\text{in}}}{\eta_{\text{buck-boost}}} = 0. \tag{3.12}$$

- **Mode 3:** This mode occurs when there is no generation from the PV side due to very low irradiance, and the battery SOC still within the operating limit. The load will be supplied only by the battery. The power balance in this mode is stated in Equation 3.13.

$$P_{\text{batt}}^{\text{out}} \cdot \eta_{\text{buck-boost}} \cdot \eta_{\text{inv}} - P_{\text{load}} = 0. \tag{3.13}$$

- **Mode 4:** This mode occurs when the battery SOC hits or surpasses the upper limit. The PV-curtail operation will be performed, and the PV generation will be lower than the load demand, hence the battery will start to discharge. The power balance in this mode is stated in Equation 3.11. The only different is the value of P_{boost}, which is determined by the PV-curtail algorithm. To avoid oscillation during the change between mode 4 and

mode 2, another logic is implemented. If the mode during previous iteration was mode 4, and the SOC is higher than 85%, PBIM still operates in mode 4 until SOC is lower than 85%.

- **Mode 5:** This mode occurs when there is no generation from the PV side due to very low irradiance, and the battery SOC is lower than the lower limit. The load will be disconnected, and all the power converters are switched off. The power fail P_{fail} can be calculated using Equation 3.14

$$P_{\text{fail}} = P_{\text{load}} \tag{3.14}$$

- **Mode 7:** This mode occurs when the battery SOC is lower than the lower limit. The load will be disconnected, and all the PV generation will be used to charge the battery until the battery SOC returns to the operating range. The power fail P_{fail} can be calculated using Equation 3.14, and the power balance in this mode is stated in Equation 3.20. To avoid oscillation during the change between mode 7 and mode 1, another logic is implemented. If the mode during previous iteration was mode 7, and the SOC is lower than 15%, PBIM still operates in mode 7 until SOC is higher than 15%.

$$P_{\text{boost}} \cdot \eta_{\text{buck-boost}} - P_{\text{batt}}^{\text{in}} = 0. \tag{3.15}$$

3.2.2. Peak Shaving

The purpose of peak shaving is to minimize the the required system capacity to supply the peak load of highly fluctuating load condition [21]. For a grid-connected PV-battery system, the battery is being charged during off-peak hours while the PV and/or the grid supply the load, and during peak-hours, the battery is discharged to met the peak load (Figure 3.9). Since the electricity fee during peak-hours is more expensive than during off-peak hours, the high electricity fee during peak-hours can be avoided, and hence the cost of energy is reduced.

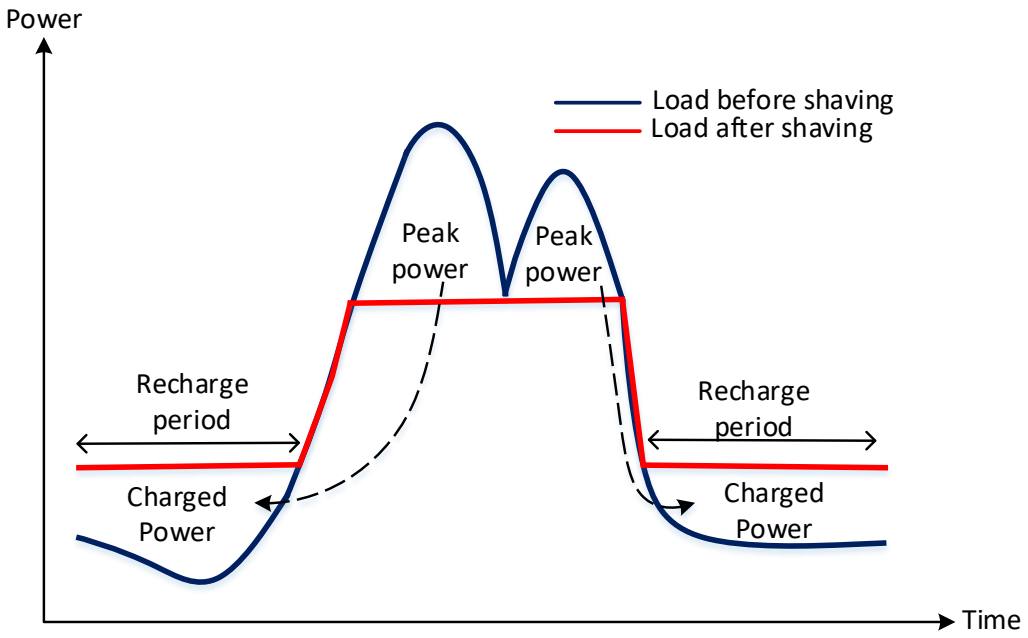

Figure 3.9: Peak shaving principle.

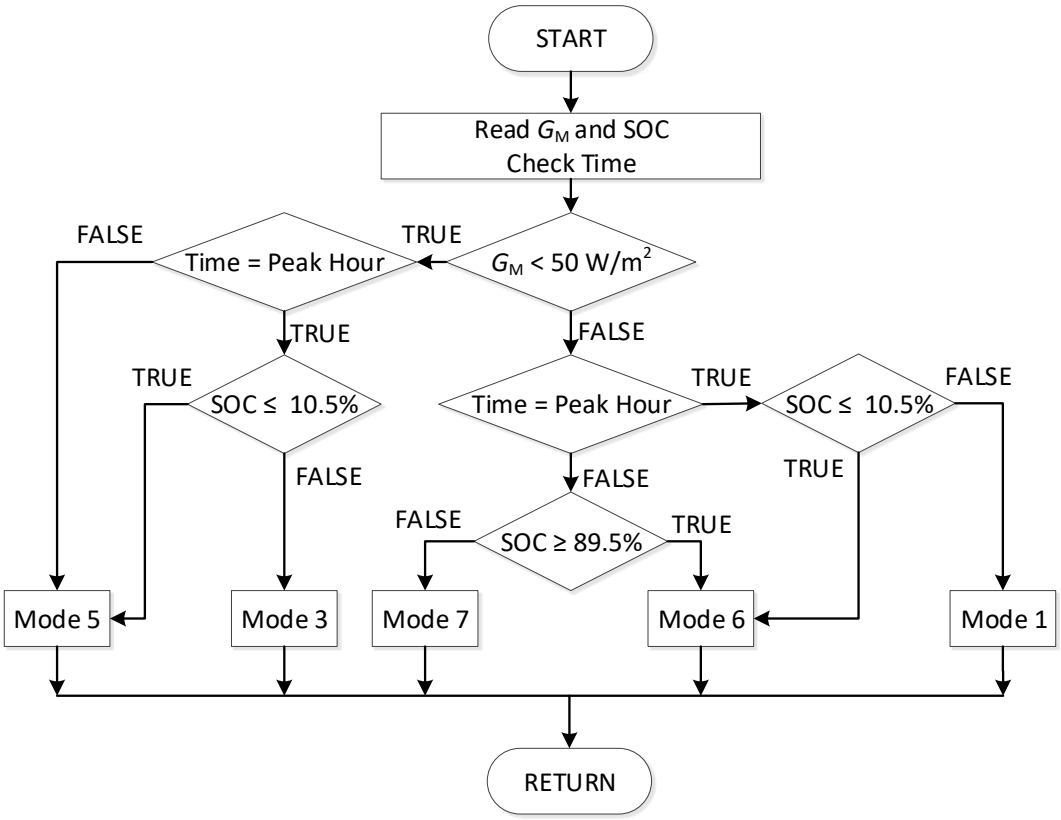

Figure 3.10: Peak shaving algorithm.

In the peak shaving algorithm, The peak hour is defined first. By checking the time and measuring the irradiance value and the battery SOC, the operation mode is determined. The minimum irradiance required to utilize the PV module is set to be 50 W/m^2. The operating limit of the battery is set to be 10.5% (lower limit) and 89.5% (upper limit). The grid power P_{grid} can be positive (drawn from the grid) or negative (supplied to the grid). There are five modes employed in the off-grid self-consumption strategy.

- **Mode 1:** This mode occurs when there is a generation from the PV side, and the battery SOC is higher than the lower limit during peak hour. The load is supplied by the PV, battery, and the grid (if necessary). Since, the battery is set to be fully discharged at the end of peak hour, the battery power is calculated using Equation 3.16, where the peak discharge current ($I_{\text{batt,peak}}$) is used. The power balance in this mode is stated in Equation 3.11.

$$P_{\text{batt}}^{\text{out}} = V_{\text{batt}} \cdot I_{\text{batt,peak}} \tag{3.16}$$

$$P_{\text{boost}} \cdot \eta_{\text{inv}} + P_{\text{batt}}^{\text{out}} \cdot \eta_{\text{buck-boost}} \cdot \eta_{\text{inv}} + P_{\text{grid}} - P_{\text{load}} = 0 \tag{3.17}$$

- **Mode 3:** This mode occurs when there is no generation from the PV side, and the battery SOC is higher than the lower limit during peak hour. The load is supplied by the battery, and the grid (if necessary). Since, the battery is set to be fully discharged at the end of peak hour, the battery power is calculated using Equation 3.16. The power balance in this mode is stated in Equation 3.11. However, the P_{boost} is zero.

- **Mode 5:** This mode occurs when there is no generation from the PV side, and the battery SOC is lower than the lower limit during peak hour. The load is supplied only by the grid. The power balance in this mode is stated in Equation 3.18.

$$P_{\text{grid}} = P_{\text{load}} \tag{3.18}$$

- **Mode 6:** This mode occurs when the battery SOC is lower than the lower limit during peak hour, or when the battery SOC is higher than the upper limit during off-peak hour. The load is supplied by the PV and the grid (if necessary. The power balance in this mode is stated in Equation 3.19.

$$P_{\text{boost}} \cdot \eta_{\text{inv}} + P_{\text{grid}} - P_{\text{load}} = 0 \tag{3.19}$$

- **Mode 7:** This mode occurs when the battery SOC is lower than the upper limit during off-peak hour. The load is supplied only by the grid, while the PV generation is used to charge the battery (if necessary). The power balance in this mode is stated in Equation 3.18 and 3.20.

$$P_{\text{boost}} \cdot \eta_{\text{buck-boost}} - P_{\text{batt}}^{\text{in}} = 0 \tag{3.20}$$

3.3. Concluding Remarks

For the grid-connected PBIM system, peak shaving strategy is useful to satisfy the load demand with minimum energy cost. Meanwhile, self-consumption method with overproduction prevention is suitable for the off-grid PBIM system. Both strategies are performed by managing the possible power flow modes in the PBIM system.

4

Modelling the PBIM System

In this chapter, the PBIM components model (PV module and battery bank) and the efficiency curve for the power electronic converters are presented. In addition, to observe the transient condition of the PBIM system using the converter control system explained in the previous chapter, MATLAB/Simulink software is used. This simulation is done to ensure that the transient time of the system is far shorter than the chosen timestep for the steady-state model simulation in the next chapter.

4.1. PV Model

PV modules parameters, such as voltage and current, can be determined by observing I-V characteristic. Also, the I-V characteristic depends on the irradiance (G_{M}) and the cell temperature (T_{M}) [17]. This section will described the mathematical model that is used to calculate the electrical parameters of the PV module. In addition, the I-V and P-V curves under various irradiances and temperatures will be shown.

4.1.1. Mathematical Model for a PV Panel

A simplified PV equivalent circuit model is used based on the single-diode PV (Figure 4.1). Since the value of shunt resistance is large, in this model, the shunt resistance is neglected by assuming the current that goes through the shunt resistance is insignificant [4]. Mathematical expressions of the PV module parameters based on this model are shown in Equation 4.1-4.7.

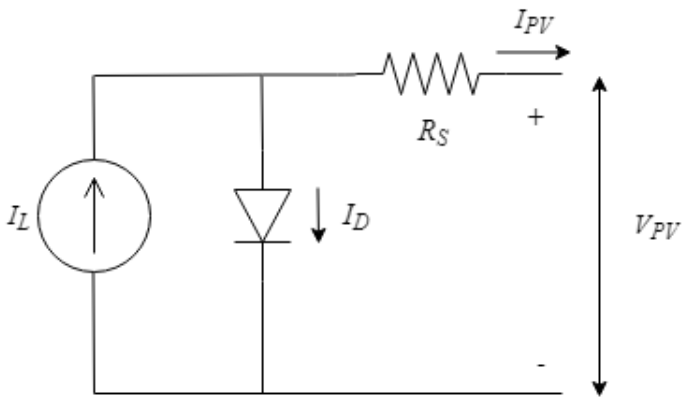

Figure 4.1: Simplified PV equivalent circuit model [4].

Standard test Condition (STC): $G_{M,STC}$ = 1000 W/m^2 and $T_{M,STC}$ = 25°C, is used as the reference to calculate the PV module electrical parameters. The electrical parameters under STC, such as open-circuit voltage ($V_{OC,STC}$), short-circuit current ($I_{SC,STC}$), max-power voltage ($V_{mpp,STC}$), max-power current ($I_{mpp,STC}$), are obtained from the datasheet, along with the temperature coefficient of V_{OC} (K_v), and temperature coefficient of I_{SC} (K_i) data.

To determine the relation between the PV voltage (V_{PV}) and the PV current (I_{PV}) (Equation 4.1), the light-generated current (I_L), the saturation current (I_0), thermal voltage (α), and the series resistance (R_S) need to be calculated.

$$I_{PV} = I_L - I_D = I_L - I_0 \left[\exp\left(\frac{V_{PV} + I_{PV}R_S}{\alpha}\right) - 1\right] \tag{4.1}$$

Under STC, the light-generated current ($I_{L,STC}$) is equal to $I_{SC,STC}$ [4]. Hence, I_L as a function of irradiance and temperature can be calculated using Equation 4.2.

$$I_L = \frac{G_M}{G_{M,STC}} \left[I_{L,STC} + K_i(T_M - T_{M,STC})I_{L,STC}\right] \tag{4.2}$$

The diode ideality factor (n), electron charge (q), Boltzmann constant (k_b are used to calculate V_{OC} under certain irradiance and temperature (Equation 4.3).

$$V_{OC} = V_{OC,STC} + \frac{nk_bT_M}{q}\ln\left(\frac{G_M}{G_{M,STC}}\right) + K_v\left(T_M - T_{M,STC}\right)V_{OC,STC} \tag{4.3}$$

Under STC, the value of thermal voltage (α_{STC}) can be calculated using Equation 4.4, where the number of cells in series (N_S) is taken into account. Also, thermal voltage (α) depends on the PV cell temperature (Equation 4.5).

$$\alpha_{STC} = \frac{k_bT_{M,STC}}{qN_Sn} \tag{4.4}$$

$$\alpha = \frac{T_M + 273.15}{T_{M,STC} + 273.15}\alpha_{STC} \tag{4.5}$$

Next, I_0 is calculated using the following equation:

$$I_0 = \frac{I_L}{\exp\left(\frac{V_{OC}}{\alpha}\right) - 1} \tag{4.6}$$

The value of R_S is calculated based on the PV module specification (Equation 4.7).

$$R_S = \frac{\alpha_{STC}\ln\left(1 - \frac{I_{mpp,STC}}{I_{SC,STC}}\right) + V_{OC,STC} - V_{mpp,STC}}{I_{mpp,STC}} \tag{4.7}$$

Finally, the output power of the PV module (P_{PV}) can be calculated using Equation 4.8.

$$P_{PV} = V_{PV}I_{PV} \tag{4.8}$$

4.1.2. PV Module Characteristics

Next, the I-V and P-V characteristics of the PV module under various irradiances and temperatures are simulated.

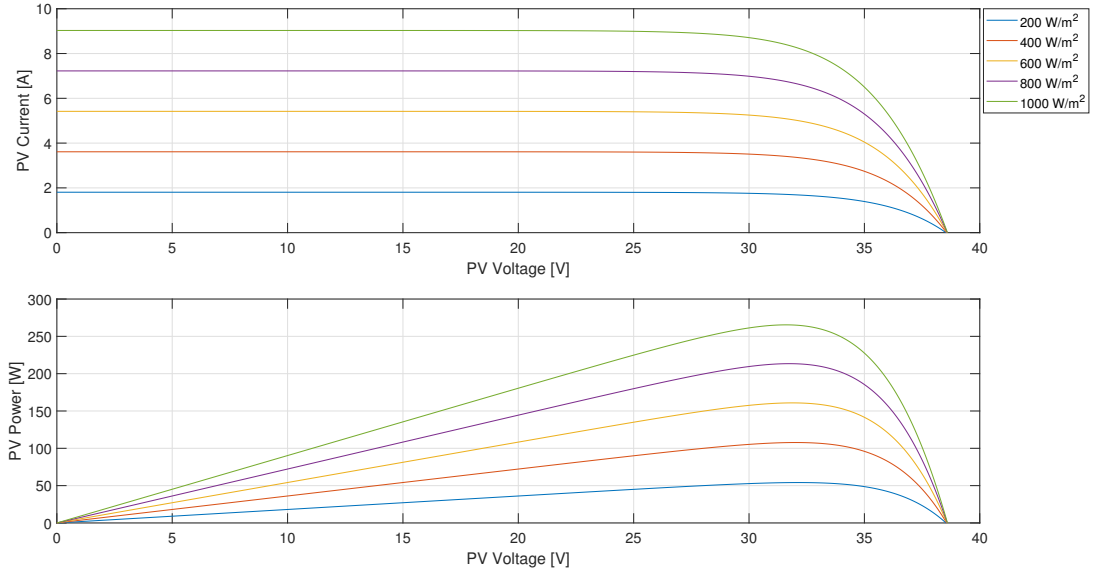

Figure 4.2: Electrical characteristics of Jinko Solar Panel JKM265P-60 at various irradiances and constant temperature.

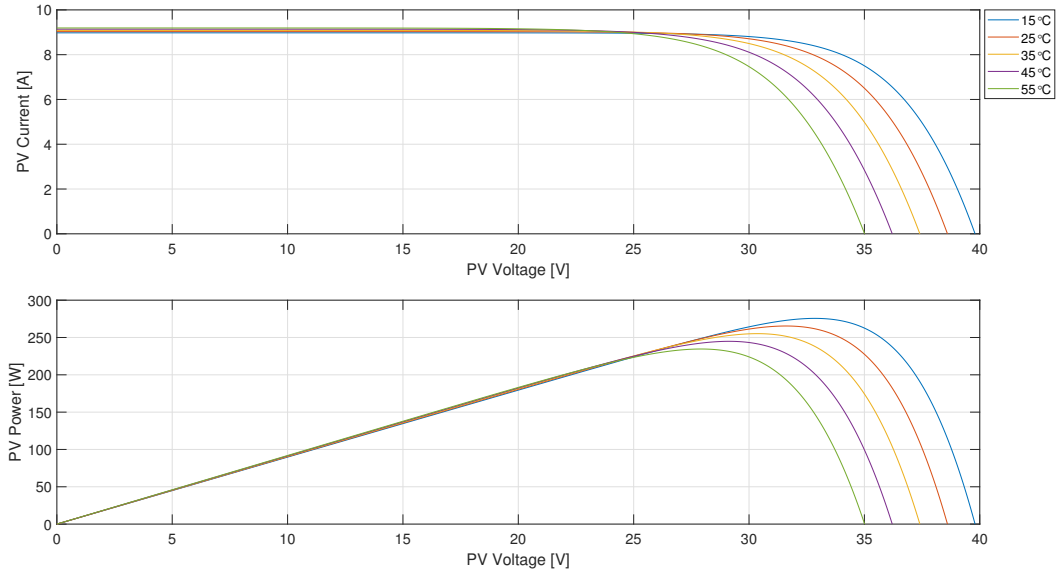

Figure 4.3: Electrical characteristics of Jinko Solar Panel JKM265P-60 at constant irradiance and various temperatures.

It is shown from Figure 4.3 and 4.2 that the change in temperature affect the V_{OC} significantly, while the change in irradiance have a little influence to the V_{OC}. On the other hand, variation in the irradiance significantly affect the I_{SC}, while insignificant change occur in the I_{SC} under various temperatures.

4.2. Battery Model

A generic battery model is developed in [22], which is also use in Solar Home System application in [23]. The output of this model are the SOC and the battery voltage as a function of battery current. The following are the mathematical equations that are used to calculate the battery SOC.

$$\mathrm{SOC}(t) = \mathrm{SOC}(t - \Delta t) + \frac{I_{\mathrm{batt}} \Delta \mathrm{t}}{Q_{\max}} \times 100\% \tag{4.9}$$

$$V_{\mathrm{cell}} = \frac{V_{\mathrm{batt}}}{N_{\mathrm{s,cell}}} \tag{4.10}$$

$$I_{\mathrm{cell}} = \frac{I_{\mathrm{batt}}}{N_{\mathrm{p,cell}}} \tag{4.11}$$

$$Q_{\mathrm{C}} = \left(100\% - \mathrm{SOC(t)}\right) Q_{\max} \tag{4.12}$$

To calculate the battery voltage, the following equations are used:
For charging ($\mathrm{I_{cell}} < 0$)

$$V_{\mathrm{cell}} = E_0 - K\frac{Q_{\max}}{Q_{\max} - Q_{\mathrm{c}}} Q_{\mathrm{c}} - K\frac{Q_{\max}}{Q_{\max} - Q_{\mathrm{c}}} Q_{\mathrm{c}} I_{cell} + A \cdot \exp(-B \cdot Q_{\mathrm{c}}) - R \cdot I_{cell} \tag{4.13}$$

For discharging ($\mathrm{I_{cell}} > 0$)

$$V_{\mathrm{cell}} = E_0 - K\frac{Q_{\max}}{Q_{\max} - Q_{\mathrm{c}}} Q_{\mathrm{c}} - K\frac{Q_{\max}}{Q_{\mathrm{c}} - 0.1 Q_{\max}} Q_{\mathrm{c}} I_{cell} + A \cdot \exp(-B \cdot Q_{\mathrm{c}}) - R \cdot I_{cell} \tag{4.14}$$

Where,
E_0 = battery constant voltage [V]
K = battery polarization voltage [V/Ah] and [ω]
$Q_{\max}$ = battery maximum capacity [Ah]
R = battery internal resistance [ω]
A = exponential voltage amplitude constant [V]
B = time constant inverse [Ah^{-1}]
Q_{c} = discharged capacity [Ah]
I_{cell} = battery current [A]

All the parameters above can be extracted from the battery datasheet. The equations to extract the parameters are explained in [23].

4.3. Transient Simulation

The transient condition of the control system is simulated in MATLAB/Simulink. The model follows the chosen architecture in Chapter 2, except that the AC load and the inverter are replaced by the DC load (constant impedance). This setup is done to simplify the simulation, and the control of the DC bus voltage and the PV voltage can be observed with ease. Figure 4.4 and 4.5 show the simplified circuit model of boost converter and bidirectional buck-boost converter respectively.

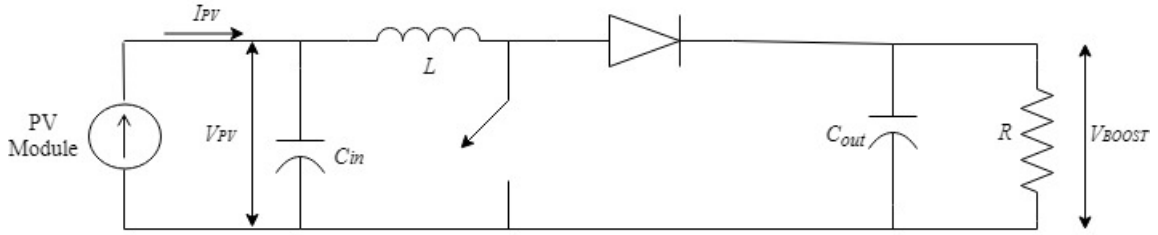

Figure 4.4: Simplified boost stage equivalent circuit model.

$$V_{\mathrm{PV}} = (1 - D_{\mathrm{boost}})\, \mathrm{V_{DC}} \tag{4.15}$$

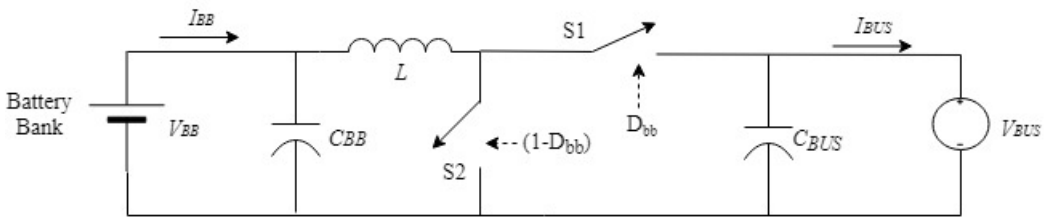

Figure 4.5: Simplified buck-boost stage equivalent circuit model.

$$V_{\mathrm{DC}} = \frac{V_{\mathrm{batt}}}{D_{\mathrm{bb}}} \tag{4.16}$$

Table 4.1 shows the parameters that are used in the simulation. The controller coefficients ($K_{p,i}$, $K_{p,v}$, $K_{i,v}$, $K_{i,i}$) are determined from trial and error method.

Parameter	**Value**	**Parameter**	**Value**
$V_{\mathrm{DC,ref}}$ [V]	48	L_{boost} [mH]	1
$V_{\mathrm{PV,mpp}}$ [V]	31.4	$L_{\mathrm{buck\text{-}boost}}$ [mH]	1
$V_{\mathrm{batt,nom}}$ [V]	26.4	$C_{\mathrm{in,boost}}$ [mF]	0.001
PV power rating [W]	265	$C_{\mathrm{out,boost}}$ [mF]	0.002
Load (nominal voltage [V], nominal load [W])	48, 200	C_{batt} [mF]	0.001
Converter switching frequency [Hz]	50000	$C_{\mathrm{DC\text{-}bus}}$ [mF]	0.002
$K_{p,v}$ [-]	0.2	$K_{i,v}$ [-]	100
$K_{p,i}$ [-]	0.02	$K_{i,i}$ [-]	100

Table 4.1: Electrical parameters for simulation.

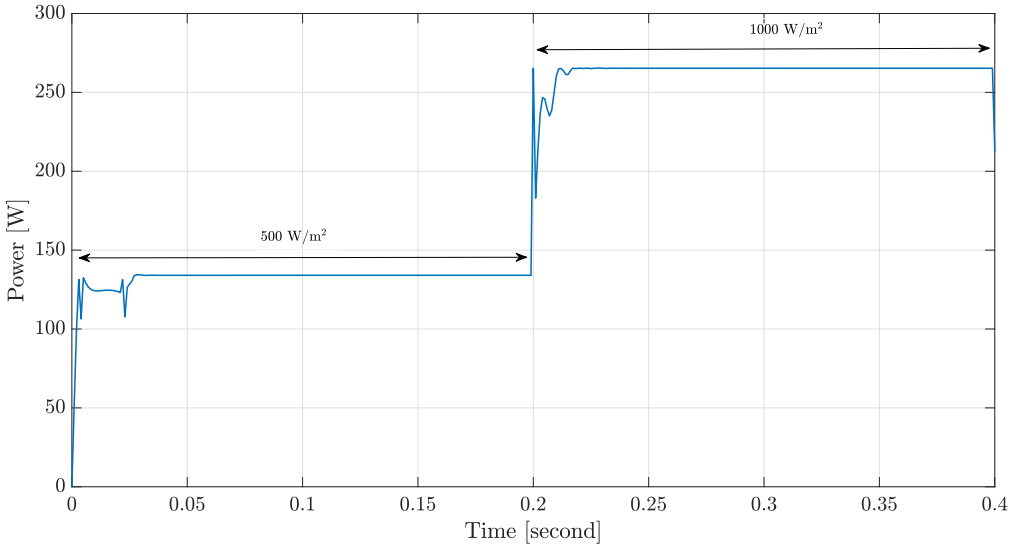

Figure 4.6: PV power.

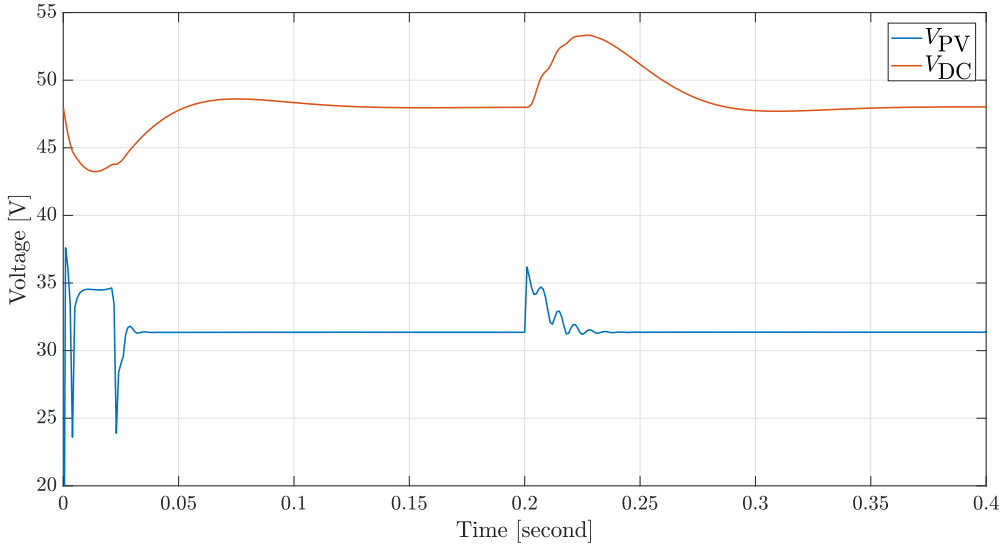

Figure 4.7: PV voltage and DC bus voltage.

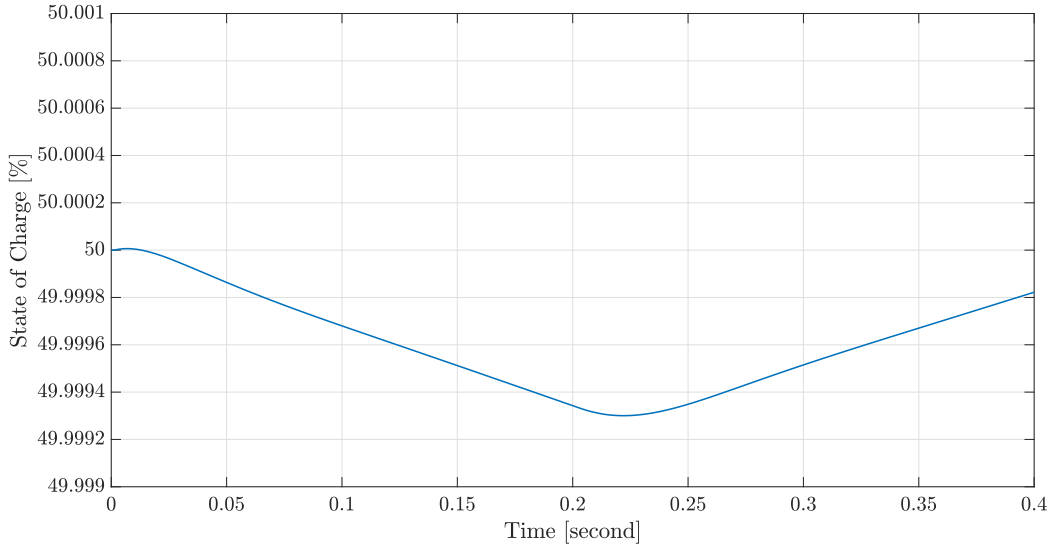

Figure 4.8: Battery SOC.

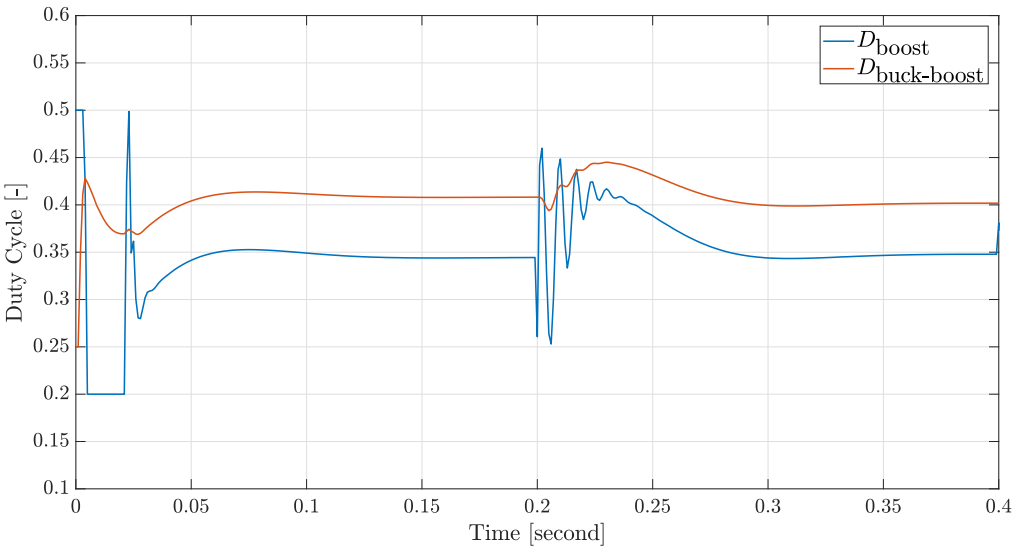

Figure 4.9: Duty Cycle.

The simulation ran for 0.4 second. The irradiance for the first 0.2 second was 500 W/m², and then it increased to 1000 W/m². First, the PV could not supply the load alone, hence the DC bus voltage decreased from its reference value. To balance the power flow in the DC bus, the battery discharged until the load is fulfilled. After the irradiance increased, the PV generation is higher than the load, hence the DC bus voltage increased from its reference value. Then, the battery is charged to store the excess power in the DC bus. It took around 0.1 second for the system to reach the steady-state condition, where the DC bus voltage does not change and has the reference value. Figure 4.6-4.9 show the PV power, the voltage, the SOC, and the duty cycle of the converters. Since the transient time is far shorter than the chosen timestep for the power flow simulation in the case study (1 minute). The transient condition is neglected in the power flow calculation and energy management strategy algorithms.

4.4. Power Electronics Efficiency

The efficiency of power electronic converter depends on the input voltage and power. An efficiency curve will be used to determine each converter input/output power, so more realistic power calculation can be performed in the energy management strategy. This section will present the efficiency curve of the converters used in the PBIM system.

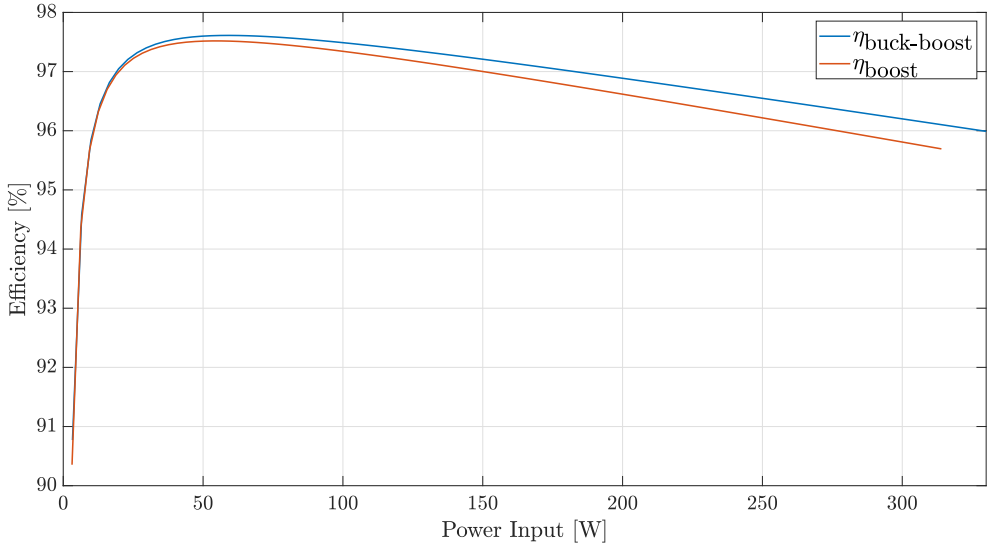

Figure 4.10: Efficiency of the unidirectional boost converter and bidirectional buck-boost converter as a function of input power.

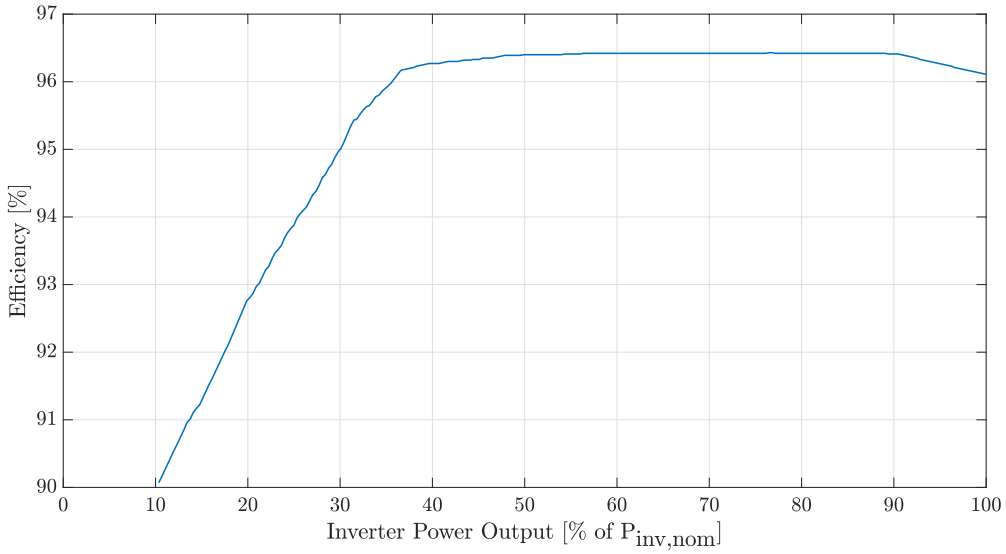

Figure 4.11: Efficiency of the inverter as a function of output power.

For the unidirectional boost converter, its efficiency will vary depending on the PV power. For the bidirectional buck-boost converter, its efficiency will vary depending on the battery power. The efficiency curves for both converters are plotted based on the loss calculation conducted in [24]. Figure 4.10 shows the efficiency curves of the unidirectional boost converter and bidirectional buck-boost converter. If the power input is lower than the lowest power input depicted in the curve, the efficiency is assumed to be the lowest value depicted

in the curve.

For the inverter, its efficiency depends on the load demand, hence the efficiency curve of the inverter is plotted as a function of output power. Figure 4.11 shows the efficiency of the inverter. This efficiency curve is obtained from the datasheet of ABB micro inverter [25]. The nominal power of the inverter ($P_{inv,nom}$) is chosen based on the PBIM application. If the power output is lower than the lowest power output depicted in the curve, the efficiency is assumed to be the lowest value depicted in the curve.

4.5. PBIM Model Overview

Figure 4.12 illustrates the PBIM model that will be used in the next two chapters. This model utilizes the PV model, the battery model, the chosen EMS (peak shaving or self-consumption), and the power electronics efficiency. The input of this model are the meteorological and load data, and the output of this model are the power flow data, the voltage of PBIM components, and the battery SOC.

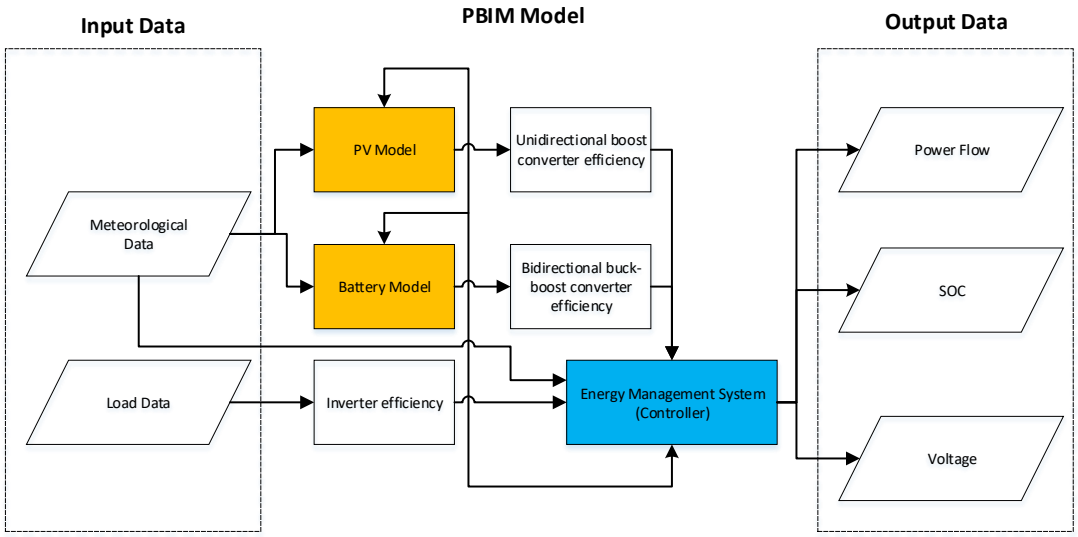

Figure 4.12: PBIM model.

4.6. Concluding Remarks

The PV model and the battery model in the PBIM system have been discussed in this section. The models can represent the electrical parameters of the components. Also, since the transient time of the controlled system is less than 0.1 second, the steady-state condition of the operation can be assumed with a time step of one minute.

5

Off-Grid PBIM in Cambodia

To analyze the performance of the PBIM system with the suitable energy management strategies, several case studies are introduced. In this chapter, the performance of an off-grid PBIM in Cambodia is observed. The implemented energy management strategies for this PBIM application is the off-grid self-consumption. This chapter presents the daily dynamic behaviour of the PBIM system and analyzes the system performance for a whole year. The chosen simulation step size is one minute. The simulation is done in MATLAB.

5.1. Location Analysis

Cambodia is a Southeast Asian country located in the tropical zone. The climate in Cambodia is heavily influenced by the annual moonsoon cycle, hence its season is alternating between dry and wet/rainy seasons. Dry season occurs during the first three months and the last three months in a year, while rainy season occurs in the middle of the year for around six months. Figure 5.1 clearly shows the different between the irradiances during dry and rainy seasons. The data for the environmental condition, such as global irradiation and ambient temperature were acquired using Metenorm for the chosen location (Stung Treng, Cambodia). The time step for all the data was 10 minutes.

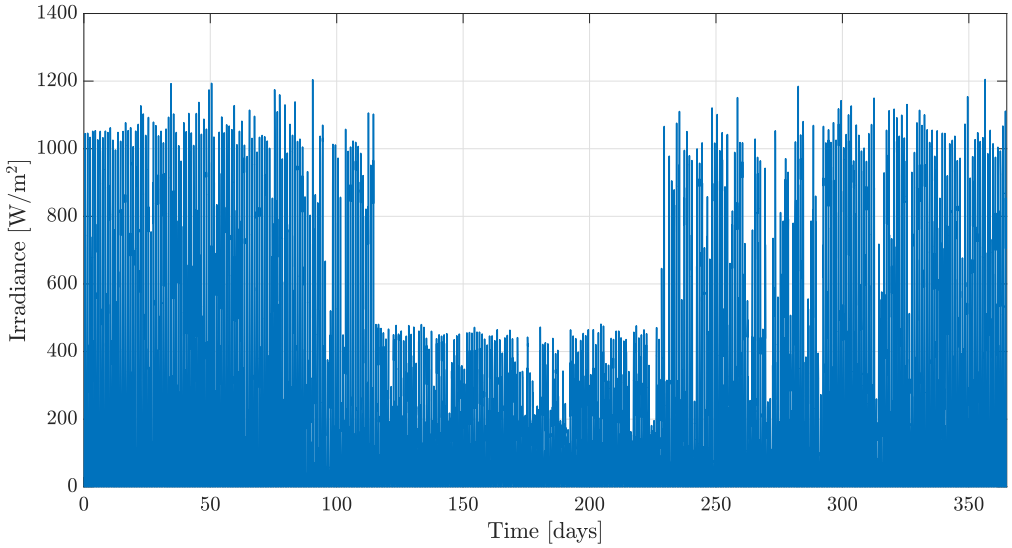

Figure 5.1: Annual PV irradiance in Cambodia.

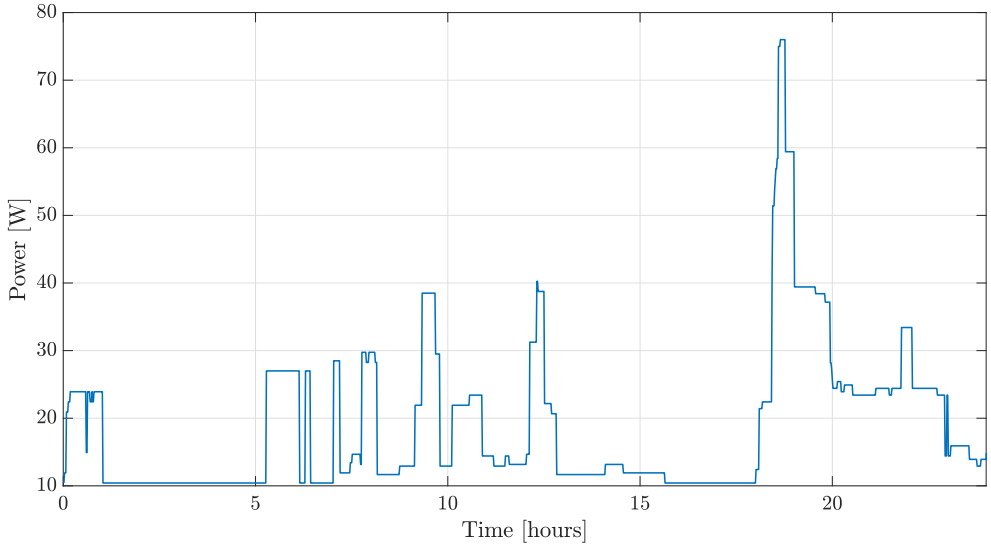

Figure 5.2: Off-grid load profile.

For this case study, the average daily load profile that represents one house hold is used (Figure 5.2), and the load varies per minute. This load profile is taken from a stochastic model developed in [26], and the value is half of the tier 3 load profile.

For observing the daily system dynamic during dry and rainy seasons, the daily data for both seasons will be used (two days for each season are selected). Figure 5.3 shows that the irradiance during dry season is significantly higher than during rainy seasons. The irradiance during dry season can reach around 1000 W/m^2, while the irradiance during rainy season can only reach around 400 W/m^2. Futhermore, the ambient and module temperature during dry and rainy seasons are presented in Figure 5.4. The ambient temperature during rainy season is slightly higher than during dry season, while the module temperature during dry season is higher than during rainy season due to big difference in the irradiance. The module temperatures were calculated using fluid-dynamic model [17].

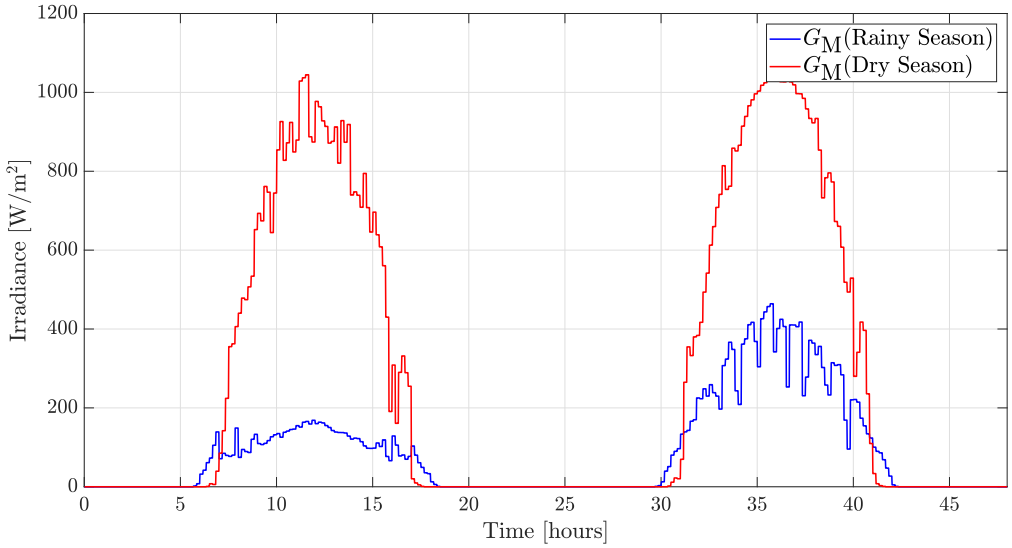

Figure 5.3: Irradiance.

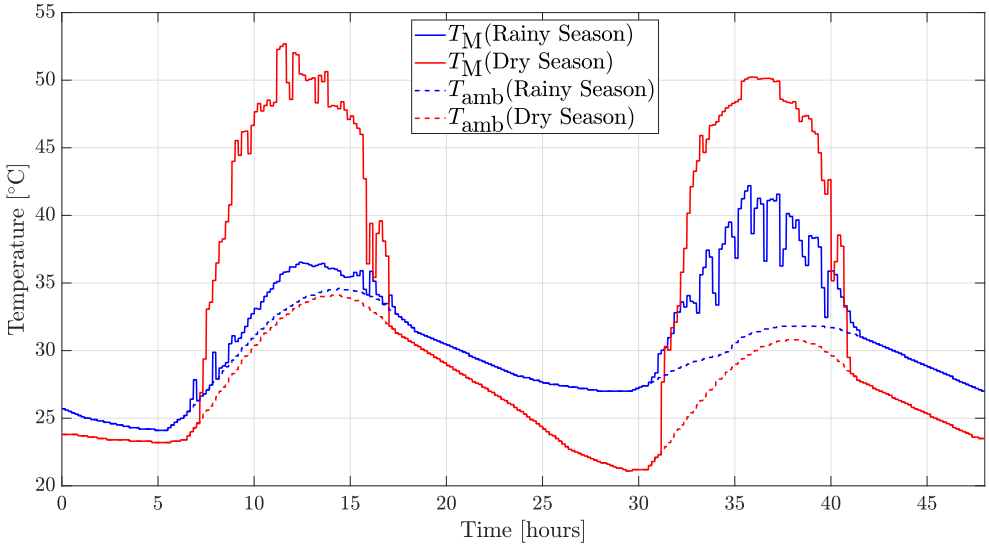

Figure 5.4: Temperature.

5.2. System Sizing

For sizing the battery capacity for the PBIM system, the LLP optimization methodology is used. The PBIM system is simulated under various battery capacity. the starting point of battery capacity is 260 Wh, which is equal to four batteries. Four batteries is chosen as the starting point due to the minimum battery voltage in the system, which is set to be 12 V. The battery capacity increment is 60 Wh, which means adding one battery to the system. The simulation end with 20 batteries (10 in series, 2 parallels), which has a maximum voltage of 36 V. Figure 5.5 shows the LLP as a function of battery capacity. The chosen battery capacity is 520 Wh (eight batteries in series), which is located around the knee point of the curve. For this battery cap city, the LLP value is 2.60% which is acceptable based on the recommended LLP for a household load [17]. The chosen inverter nominal power is 300 W since the load is lower than the PV power rating. Also, only one PV module is used in this case study. Hence, the PBIM system in Cambodia will consists of one PV module and eight batteries in series.

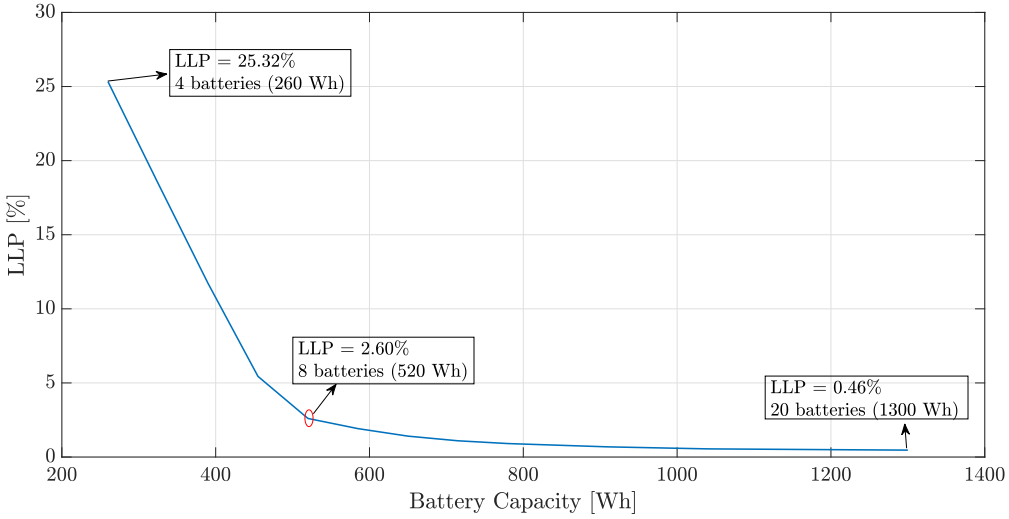

Figure 5.5: Loss of load probability as a function of battery capacity.

5.3. Daily System Dynamic

In this section, the daily system dynamic of the PBIM system is analyzed. First, the power flows for both dry and rainy seasons are discussed. In addition, the modes of operation during two days simulation are observed. Next, the PV voltage and the battery voltage during dry and rainy seasons are compared. Finally the battery SOC variation is discussed. The initial battery SOC for both seasons are 10%.

5.3.1. Power Flow and Modes of Operation

Two days simulation is performed for both dry and rainy seasons. Figure 5.6 and 5.7 show the results of the PBIM system dynamic for both seasons. For the battery power, positive sign means the battery is discharging, while negative sign means the battery is charging.

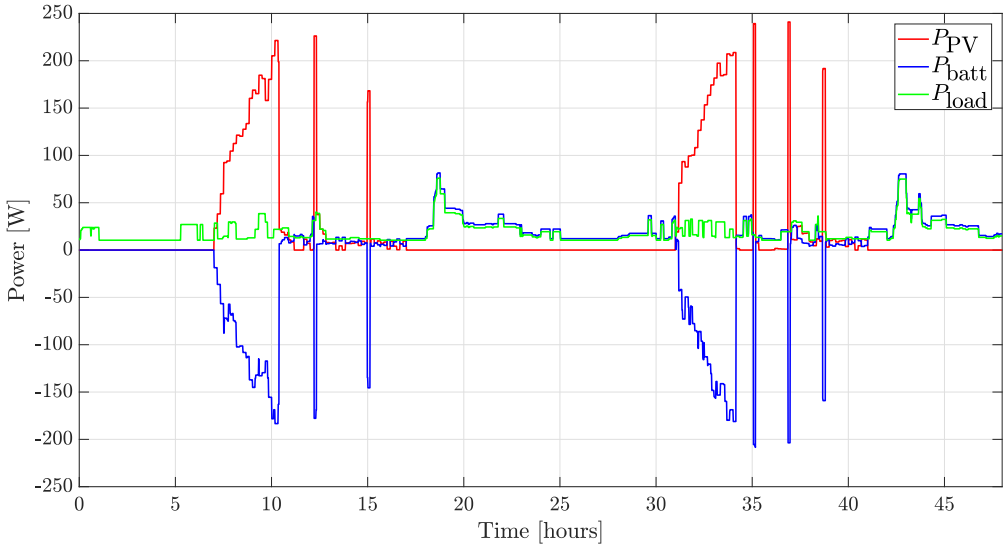

(a) Power flow.

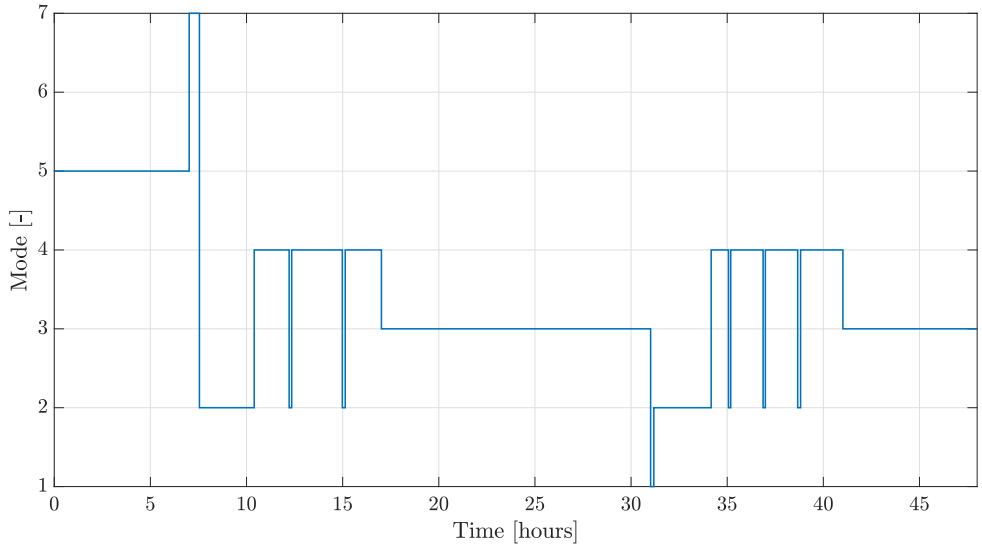

(b) Mode of operation.

Figure 5.6: Dry season.

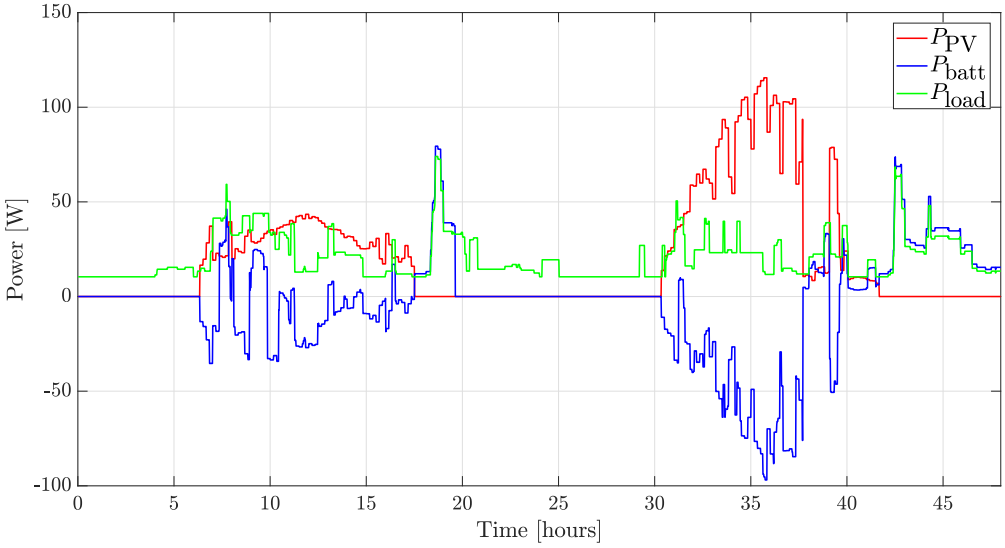

(a) Power flow.

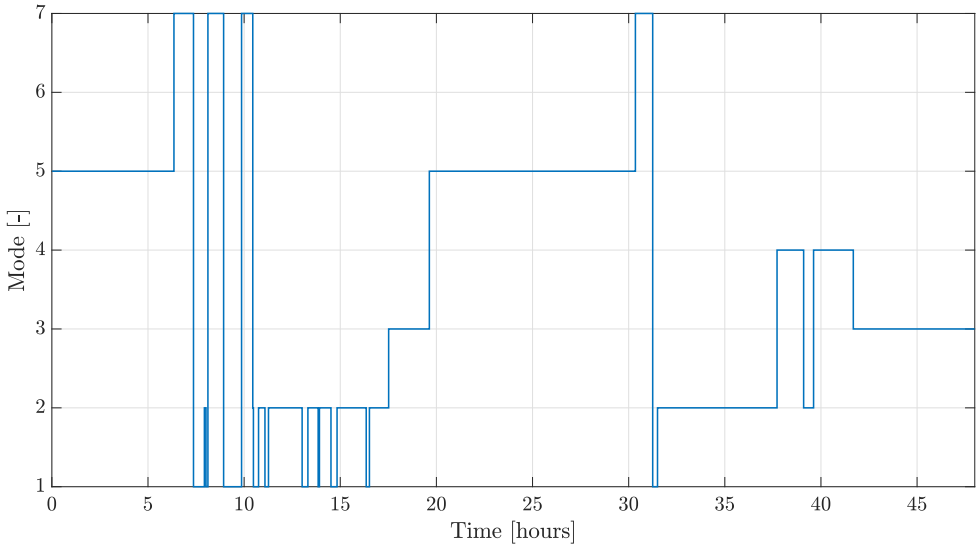

(b) Mode of operation.

Figure 5.7: Rainy season.

Dry Season

At the beginning of day one, the PBIM is operating in mode 5 since the battery SOC is 10% and there is no PV generation. During this mode, the load is disconnected and power fail is occured. Around 7-8 AM, the PV starts to generate power. The PBIM operates in mode 7 to charge the battery since the SOC is lower than 10%. Mode 1 occurs during small period after the SOC is higher than the lower limit since the PV cannot supply the load alone. From 8 AM until around 11 AM, the PBIM operates in mode 2 due to the increase in the irradiance, and the battery starts being charged. Around 10 AM , the battery SOC hits the upper operation limit. Since The irradiance is still high, the PBIM starts to operate in mode 4 to curtail the PV power to avoid power dump. In the afternoon, the PBIM operates between mode 2 and mode 4, which is reflected in 5.6. Around 6 PM, since the sun is set, mode 3 occurs. In the night, the PBIM operates in mode 3 since there are no PV generation to supply the load. In this situation, the battery is discharging.

Rainy Season

At the beginning of day one, the PBIM is operating in mode 5 since the battery SOC is 10% and there is no PV generation. During this mode, the load is disconnected and power fail is occured. Around 7-8 AM, the PV starts to generate power. The PBIM operates in mode 7 to charge the battery since the SOC is lower than 10%. Since the irradiance is lower during rainy season compared to during during dry season, hence the PBIM rarely operates in mode 4. During the day, the PBIM operates between mode 2 and 1. In the night, mode 3 occurs. For the second day, since the battery SOC does not start from 10%, mode 4 occurs in the afternoon, and the PBIM starts to operate between mode 2 and mode 4.

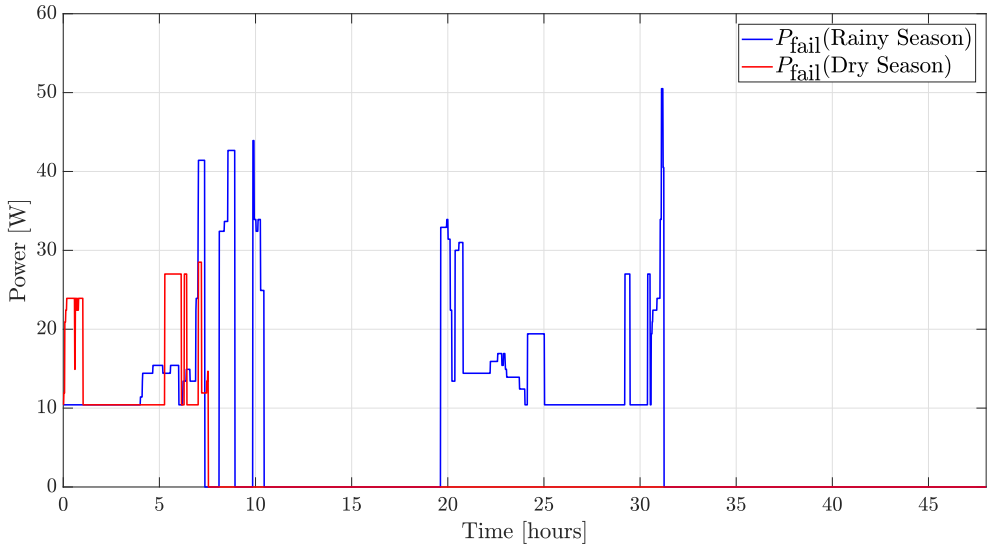

Figure 5.8: Power fail during dry and rainy seasons.

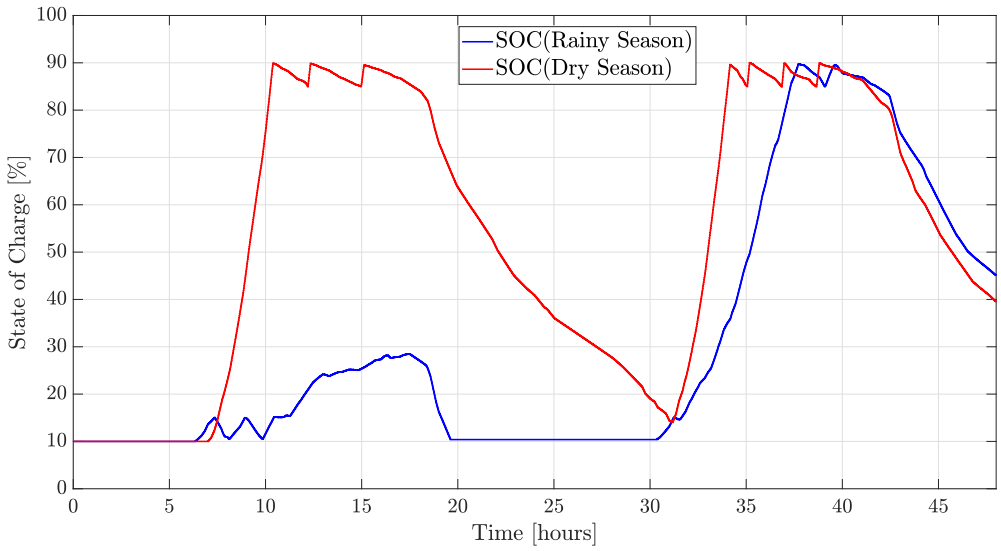

Figure 5.9: Battery bank SOC for two days simulation.

Battery State of Charge

Figure 5.9 shows the SOC variation for both seasons. During dry season the SOC always hit the upper limit in the afternoon, and never hit the lower limit at the end of the day. At

the end the day, the SOC is around 20-30%. On the contrary, during rainy season, the SOC does not hit the upper limit in the afternoon. Also, the SOC hits the lower limit in the night of day one.

Power Fail

Figure 5.8 presents the power fail during dry and rainy seasons. It can be seen that the power fail during dry season only occurs in the beginning of day one, since the initial SOC is 10%. Meanwhile, the power fail occurs in the beginning of day one and two, and during the night of day one. This is caused by the big difference of irradiance between these two seasons.

5.3.2. PV and Battery Voltages

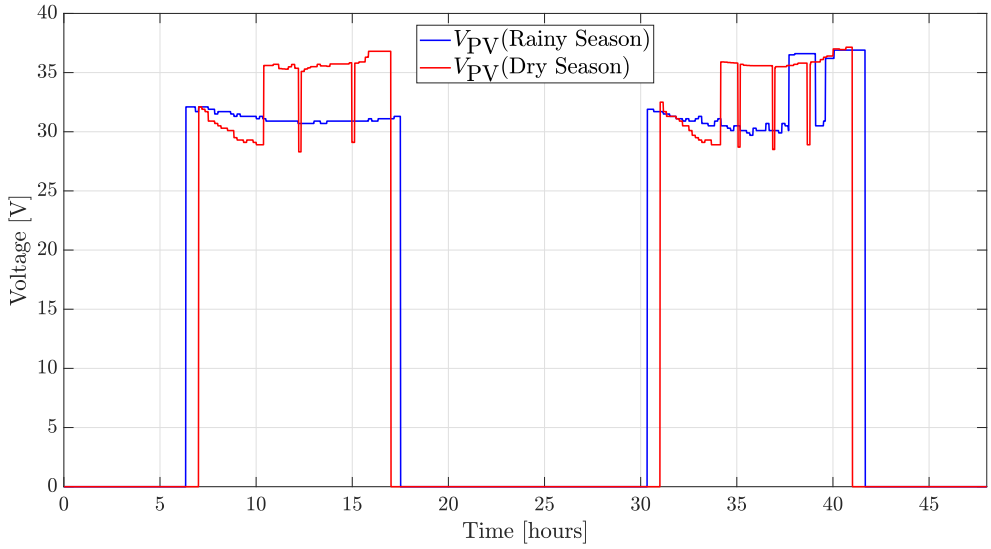

(a) PV voltage.

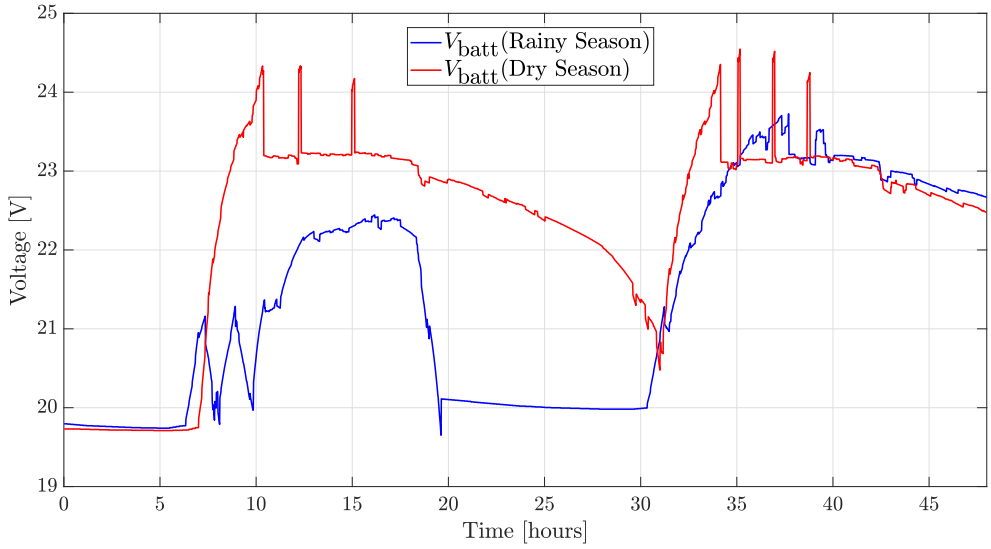

(b) Battery Voltage.

Figure 5.10: Voltage of the PBIM components.

Figure 5.10 shows the voltage of the PBIM components. It can be seen that during dry season, the PV voltage highly fluctuates compared to rainy season since the PV curtail operation is performed, while the MPPT operation is performed during rainy season most of the time. For the battery voltage, its value is fluctuating during the afternoon of dry season because the battery switches between charging and discharging operation. On the other hand, the battery voltage during rainy season does not fluctuate highly.

5.4. Yearly System Performance

In this section, the montly LLP of the PBIM system, the reduction of PV generation due to PV-curtail algorithm, and the energy exchange in the system are discussed.

5.4.1. Loss of Load Probability

Figure 5.11 shows the monthly LLP of the PBIM system. During the beginning of the year (Jan-Mar), the load demand is fulfilled by the PBIM system most of the the time since the LLP is lower than 1%. Then, the LLP is increasing as the dry season ends, and the rainy season starts (Mar-Sep). The LLP during the middle of the year vary around 2% to 7%. After the rainy season ends, the LLP decreases again until the end of the year (Sep-Dec). This result means that the PBIM system is well-sized to handle the load during rainy and dry seasons since the LLP never reach 10% for every month.

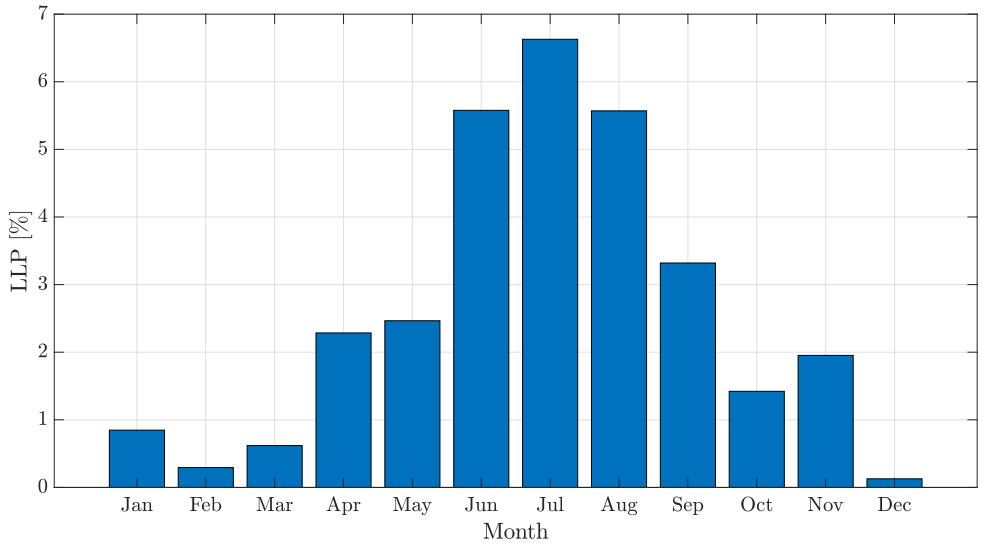

Figure 5.11: Monthly Loss of Load Probability.

5.4.2. Reduction of PV Generation

Figure 5.12 presents the PV generation comparison between the control system with only MPPT algorithm and the control system with MPPT and PV-curtail algorithms. It can be seen that the latter kept the PV generation from exceeding the required load demand and the available battery capacity through the whole year. Figure 5.13 shows the percentage of curtailed PV generation for every month. During dry season, the PV generation needs to be reduced by 55-62% to avoid power dump. Meanwhile, the PV generation have to be reduced by 10% during rainy season.

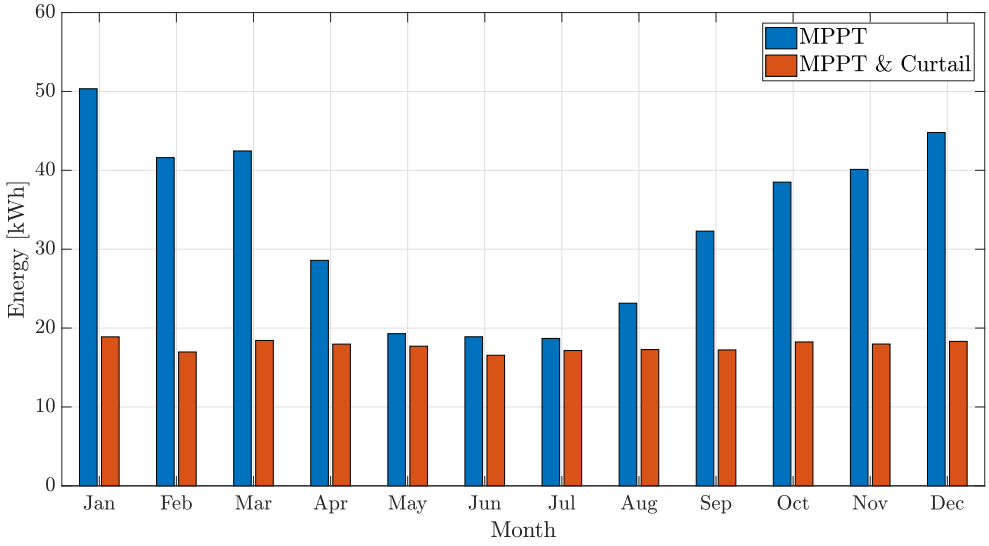

Figure 5.12: Monthly PV generation.

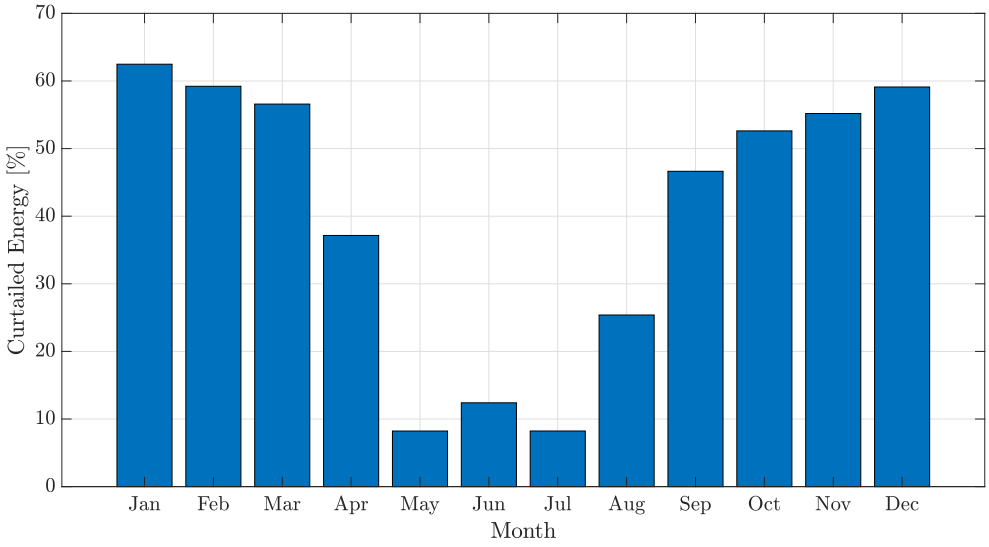

Figure 5.13: Monthly curtailed energy.

5.4.3. Energy Exchange

The energy exchange in the PBIM system is presented in Figure 5.14. The total energy generated from the PV module is 212.71 kWh. The losses in the system is around 17% of the PV generation (37.58 kWh). From the annual load demand of 179.11 kWh, the total load that is fulfilled is 174.45 kWh, while the remaining 4.66 kWh is not supplied by the system. At the end of the year, the energy that is stored to the batter is 0.67 kWh.

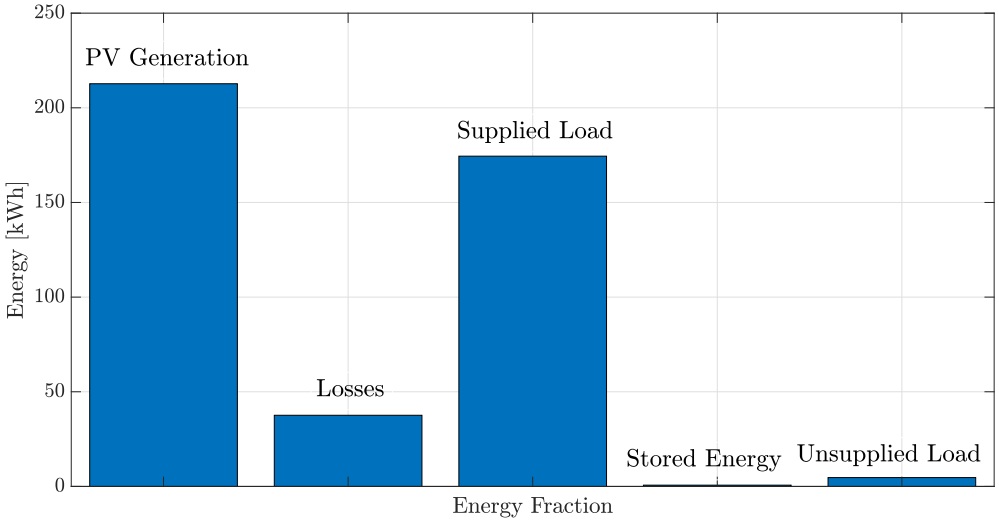

Figure 5.14: Yearly energy exchanged by the off-grid PBIM system.

5.5. Constant Load

In this section, the PBIM is given a constant load at 90 W, which represents an LCD TV [27]. This is done to observe the behaviour of PBIM operation under constant load. The irradiance and temperatures have the value like in section 5.1, but only for the first day. The simulation is done for one day. Figure 5.15-5.18 show the behaviour of the PBIM system. It can be seen the the PBIM can supply the load for 12 hours without failing. This means that PBIM can be used as emergency option to supply a certain load.

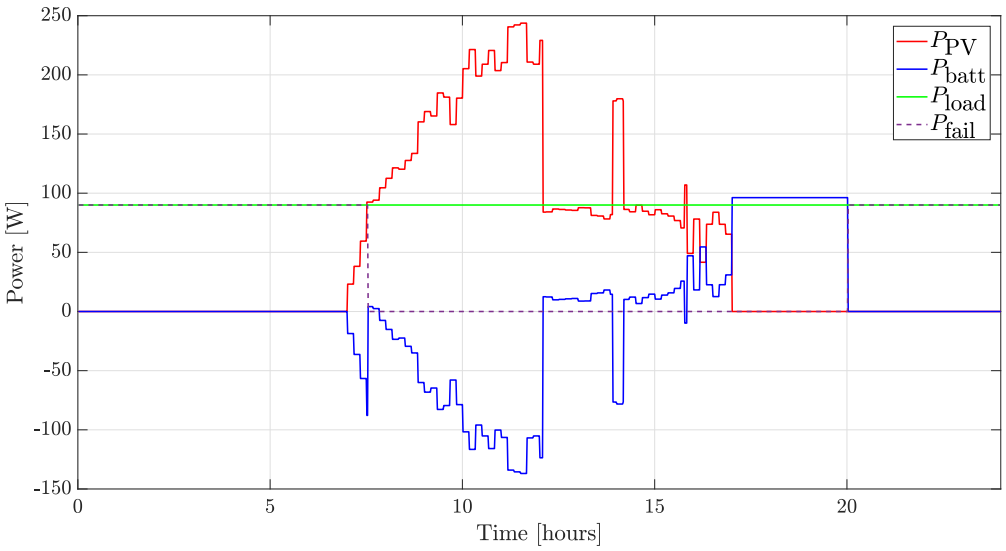

Figure 5.15: Power Flow.

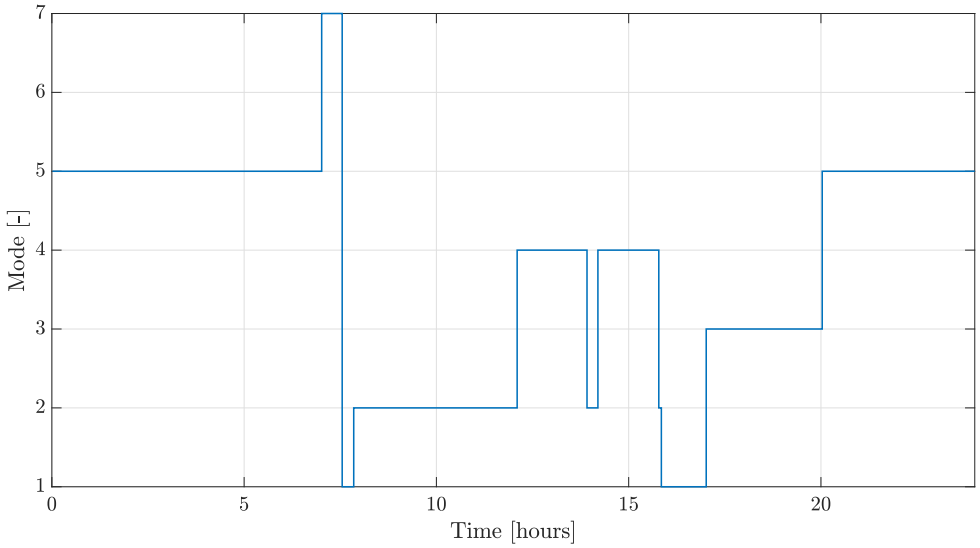

Figure 5.16: Mode of Operation.

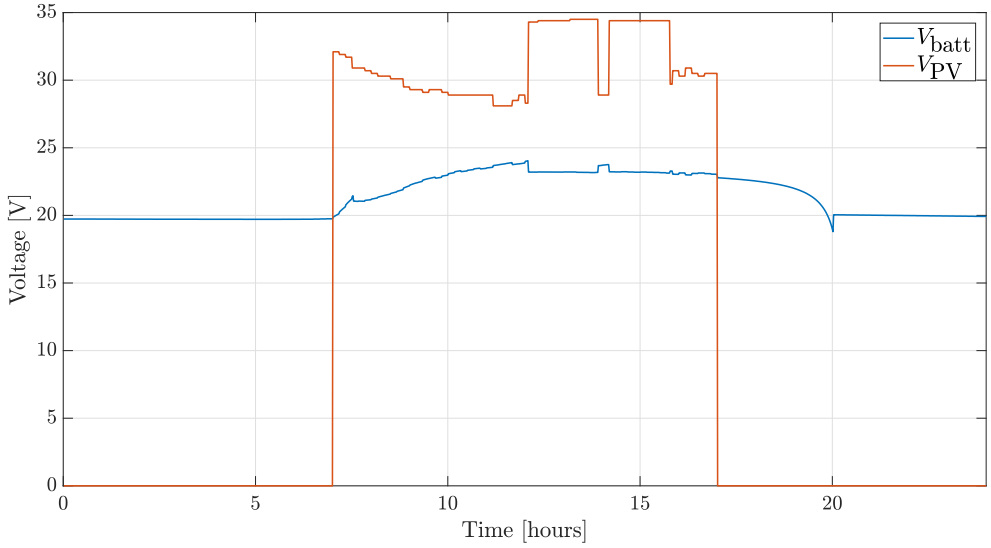

Figure 5.17: Voltages.

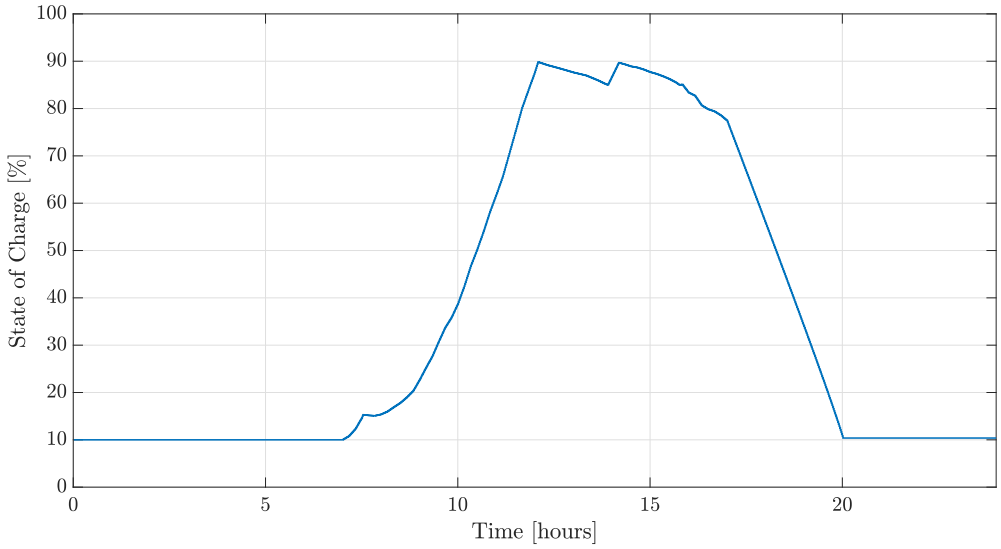

Figure 5.18: Voltages.

5.6. Concluding Remarks

Case study for an off-grid PBIM in Cambodia is conducted. The results show that the PBIM system has a good performance during dry and rainy seasons. The implemented energy management strategy performs well, which reflected by keeping the SOC within limit and curtailing the PV generation when there is an excess energy.

6

Grid-Connected PBIM in the Netherlands

In this chapter, the performance of a Grid-connected PBIM in the Netherlands is observed. The implemented energy management strategies for this PBIM application is the peak shaving. This chapter presents the daily dynamic behaviour of the PBIM system and analyzes the system performance for a whole year. The chosen simulation step size is one minute. The simulation is done in MATLAB.

6.1. Location Analysis

The data for the environmental condition, such as global irradiation and ambient temperature were acquired using Metenorm for the chosen location (Delft, the Netherlands). The time step for all the data was 1 minute. Figure 6.1 shows the annual irradiance in Delft. Figure 6.2 shows the daily household load variation in the Netherlands, which is obtained from [28].

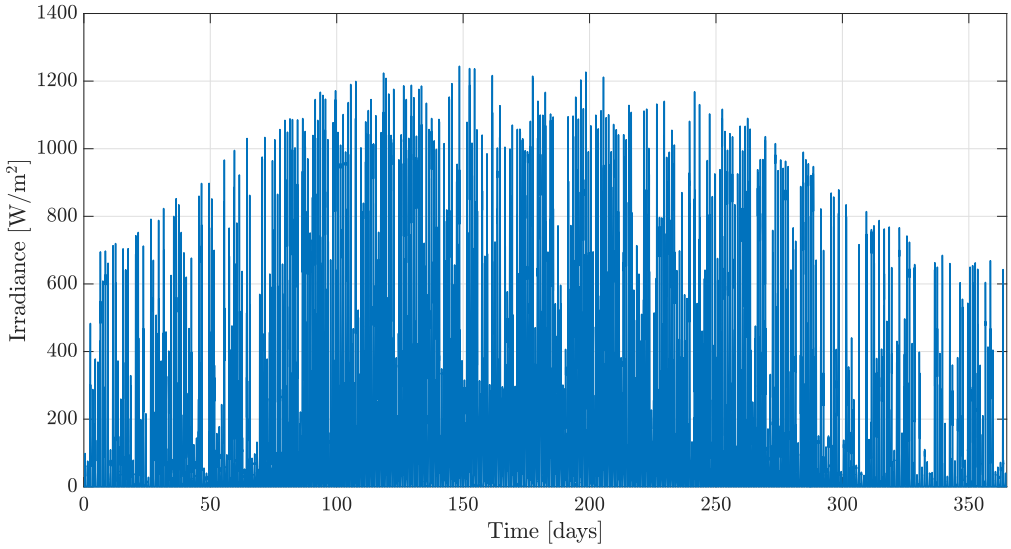

Figure 6.1: Annual irradiance in the Netherlands (Delft).

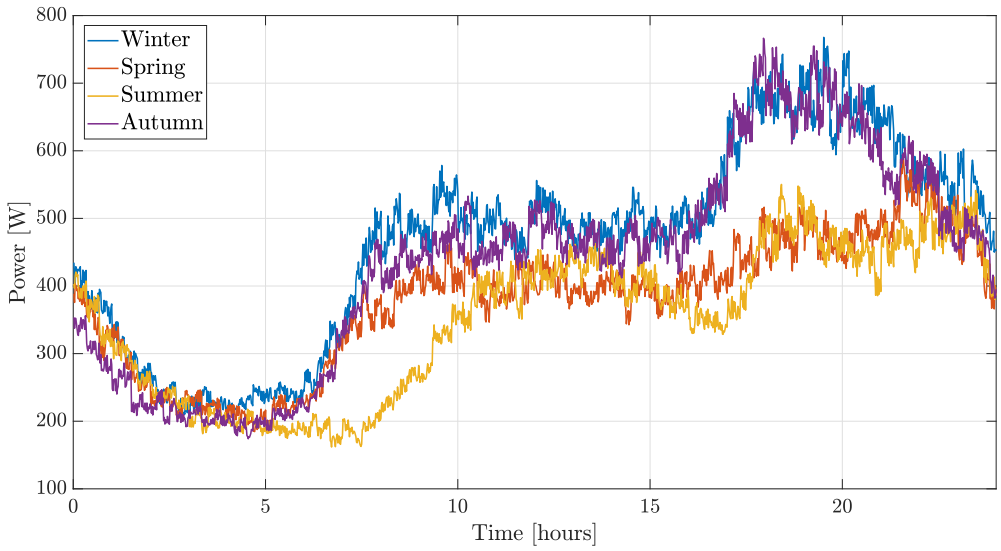

Figure 6.2: Daily load variation in the Netherlands.

6.2. System Sizing

For sizing the battery capacity for the PBIM system, the energy drawn from the grid during peak hours under various battery capacity are observed. The starting point of battery capacity is 260 Wh, which is equal to four batteries. Four batteries is chosen as the starting point due to the minimum battery voltage in the system, which is set to be 12 V. The battery capacity increment is 60 Wh, which means adding one battery to the system. The simulation end with 20 batteries (10 in series, 2 parallels), which has a maximum voltage of 36 V. Figure 6.3 shows the energy drawn from the grid as a function of battery capacity. Since there is no knee point between the simulated battery capacity, the chosen battery capacity is 520 Wh (eight batteries in series) which is similar with the sizing of the off-grid PBIM in Cambodia. The chosen inverter nominal power is 300 W since the battery power during peak hour is always less than 300 W for the chosen sizing, and this nominal power is higher than the PV power rating. Also, only one PV module is used in this case study. Hence, the PBIM system in the Netherlands will consists of one PV module and eight batteries in series.

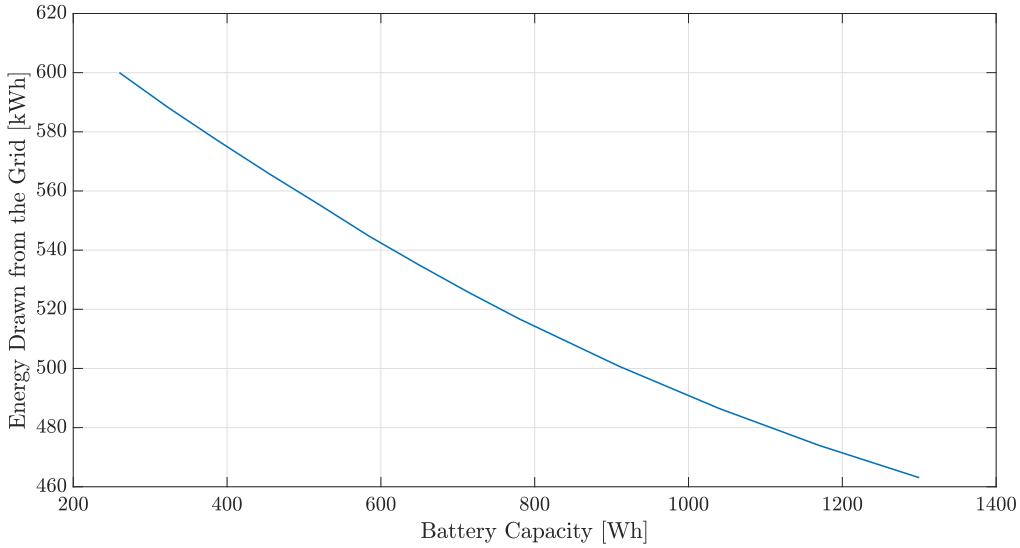

Figure 6.3: Annual energy drawn from the grid during peak hours on various battery capacity.

6.3. Daily System Dynamic

In this section, the daily system dynamic of the PBIM system is analyzed. First, the power flows for the summer days are discussed. In addition, the modes of operation during two days simulation are observed. Next, the PV voltage and the battery voltage these two days are presented. Finally the battery SOC variation is discussed. The initial battery SOC for the simulation is 10%. Figure 6.4 and 6.5 shows the irradiance and the temperatures during two days in Summer respectively.

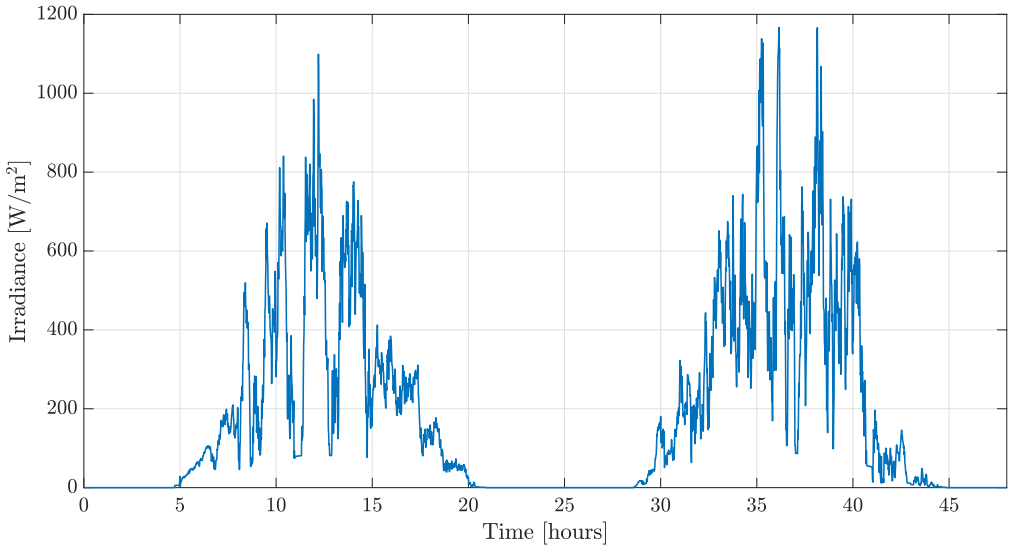

Figure 6.4: Irradiance.

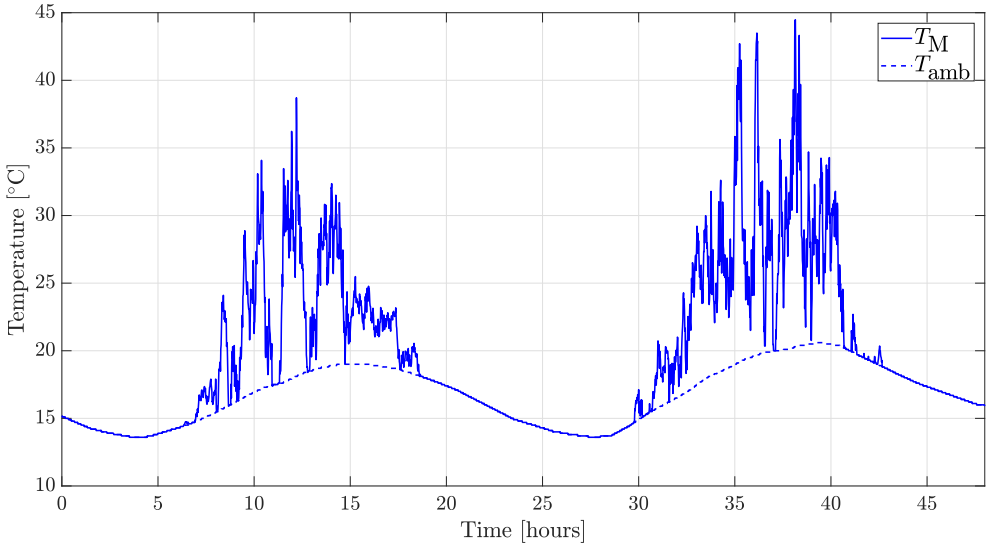

Figure 6.5: Temperature.

6.3.1. Power Flow

Figure 6.6 shows the power flow during two days simulation, while Figure 6.7 presents the mode of operation. For the grid power, positive sign means drawing energy from the grid, while negative sign means supplying to the grid. For the battery power, positive sign means

discharging operation, while negative sign means charging operation. The duration of the peak hours is four hours, and it starts from 5 PM until 8 PM.

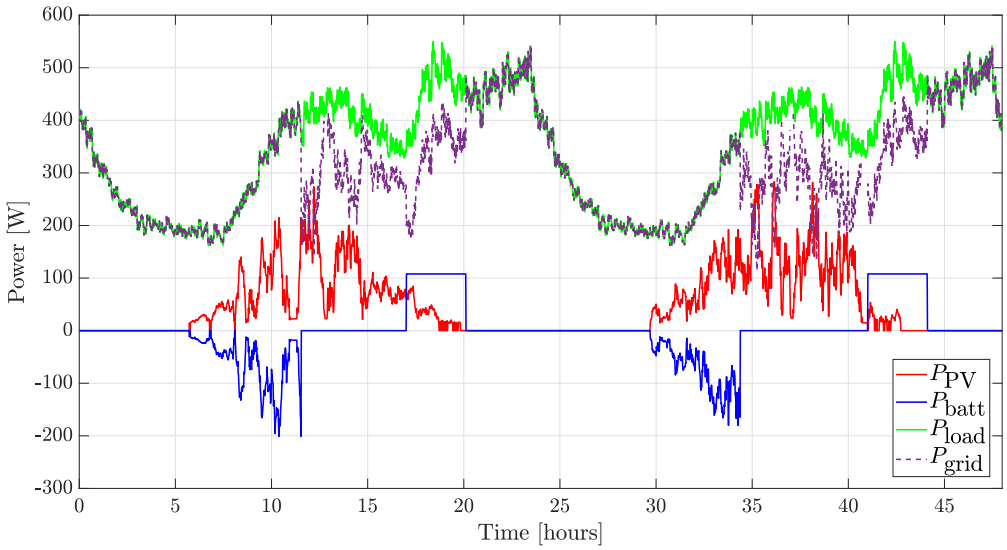

Figure 6.6: Power flow.

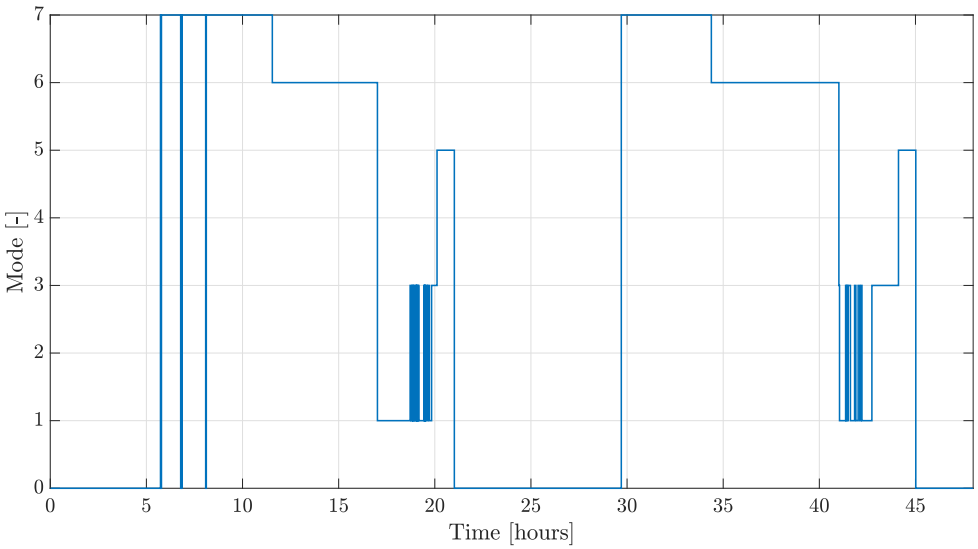

Figure 6.7: Mode of operation.

At the beginning of the day, PBIM is not operating since there is no energy stored in the battery and no PV generation, hence the load is supplied by the grid. Mode 5 and Mode 0 in Figure 6.7 represent off condition of the PBIM. After the sun is rising the PV starts to charge the battery, which means mode 7 is performed. The fluctiation behaviour between mode 7 and mode 0/5 is due to the low irradiance value (which near the lowest operating limit of irradiance). After the battery is full, the PV starts to help the grid supplying the load, which means mode 6 is performed. In this condition, the battery is disconnected, so it can be used fully during peak hours. When the peak hours start, the battery and the PV start to supply load, and since the load is much a higher than the PBIM power generation, the grid has to supply the load as well (Mode 1). The fluctuating behaviour between mode 1 and 2 is due to the irradiance.

6.3.2. PV and Battery Voltages

Figure 6.8 and 6.9 show the voltage of the PV and the battery respectively. It can be seen that the MPPT mode is always on when the PV is connected, hence the voltage always near the maximum power point. Regarding the battery voltage, a constant voltage is occurs when the battery is full during off-peak hours, then the voltage gradually decrease during peak hours, which represents discharging operation.

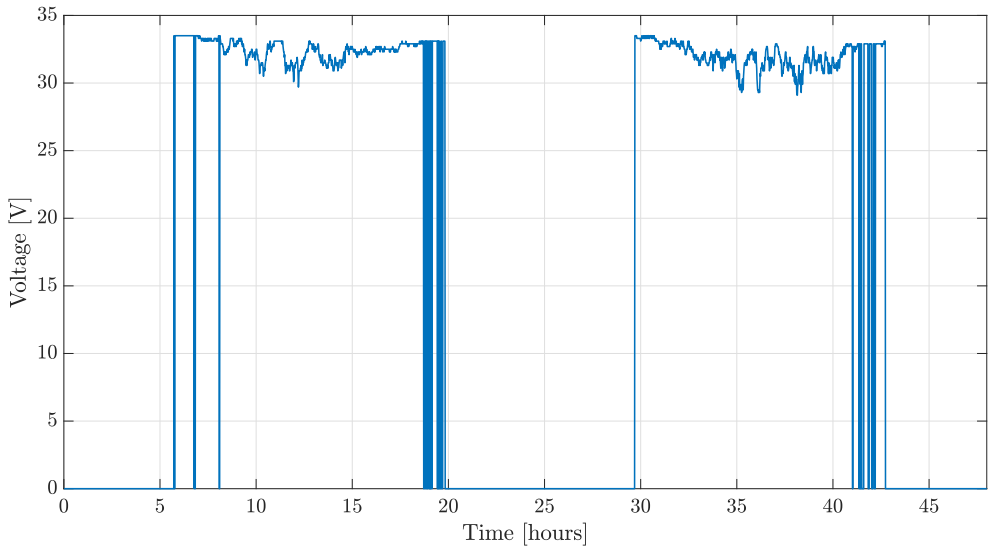

Figure 6.8: PV Voltage.

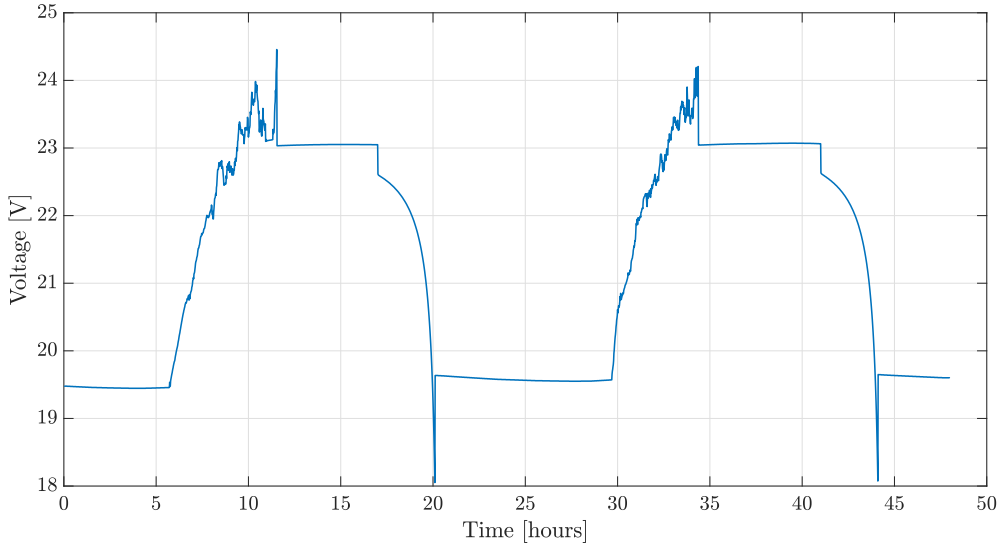

Figure 6.9: Battery Voltage.

6.3.3. Battery State of Charge

Figure 6.10 shows the SOC variation for two days simulation. During off-peak hours, the battery is being charged until it reach the maximum SOC. After that, the SOC stays at 90% until the beginning of peak hours. During peak hours, the SOC is decreasing until it reaches the minimum SOC.

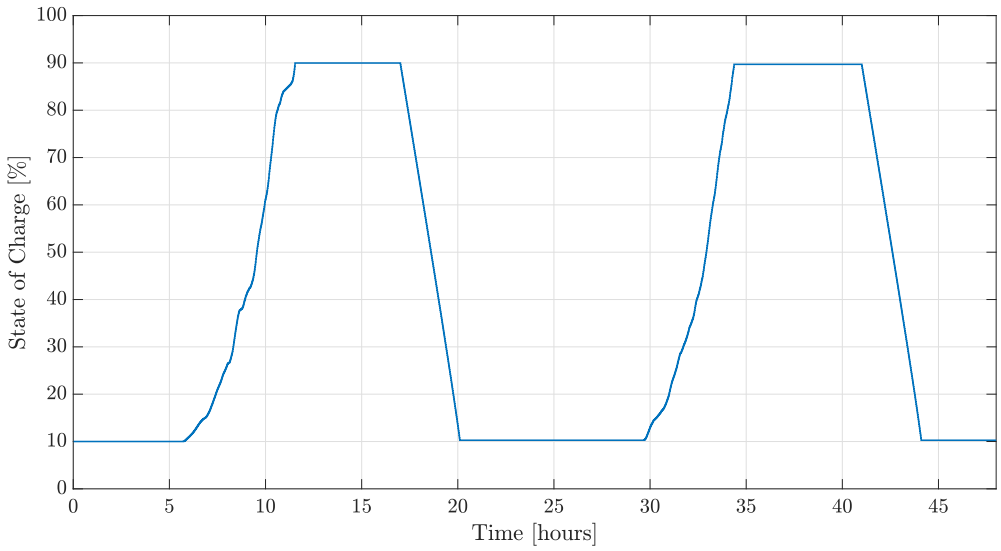

Figure 6.10: Battery bank SOC.

6.4. Monthly System Autarky

The system autarky represents the percentage of the total load demand that is successfully supplied using the energy generated from the PBIM system, which can be calculated using the following equation:

$$\text{Autarky} = \frac{\text{Energy delivered from the PBIM system during peak hours}}{\text{Total load demand during peak hours}} \times 100\% \tag{6.1}$$

Figure 6.11 shows the montly system autarky during peak hours. The monthly system autarky varies between 6-16%, where the lowest value occurs during winter, and the highest value occurs during summer. To provide better system autarky, the number of batteries per PBIM should be increased, or multiple PBIMs should be installed.

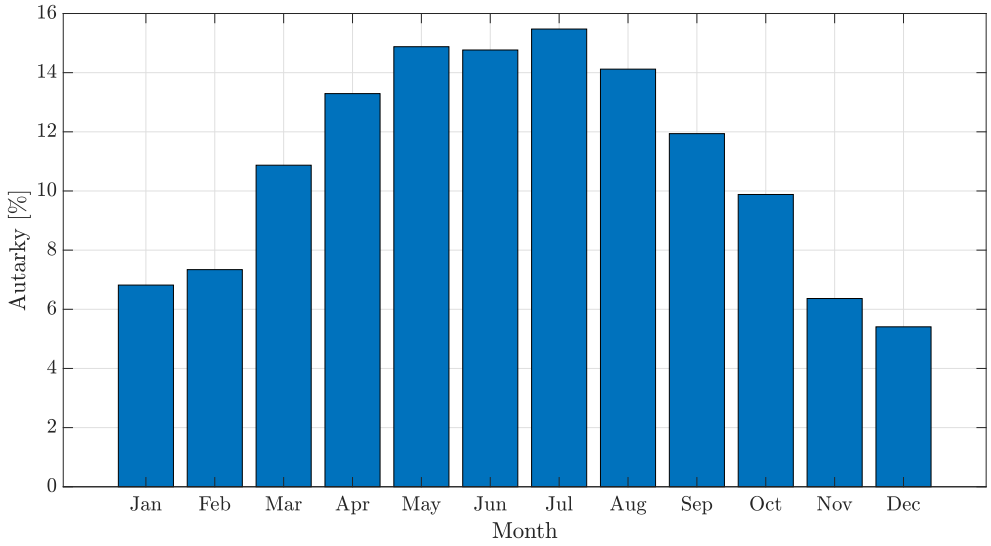

Figure 6.11: Monthly system autarky.

6.5. Concluding Remarks

Case study for a Grid Connected PBIM in the Netherlands is conducted. The results show that the system always needs energy drawn from the grid. During the peak hours, the system utilizes all the energy stored in the battery, hence less energy is drawn from the grid. During off-peak hour, the PV focuses on charging the battery, while the load is supplied by the grid. The monthly system autarky shows that one PBIM can only supply a maximum 16% of the load demand during peak hours in the Netherlands.

7

Conclusions & Recommendations

In this study, two energy management strategy for PBIM system have been implemented, namely off-grid self-consumption and peak shaving. After discussing the necessary control mechanism to implement each energy management strategy in the chosen PBIM system architecture, two case studies have investigated the performance of PBIM system. The first case study is the off-grid PBIM in Cambodia, and the second case study is the grid-connected PBIM in the Netherlands.

7.1. Conclusions

There are four main research questions have been addressed in the previous chapters.

1. **What is the suitable system architecture for the PBIM system considering the control complexity?** The chosen PBIM system architecture is the DC couple architecture. This because DC couple architecture provides sizing flexibility and safety to the battery since a bidirectional converter is utilized between the battery and the DC bus. The DC bus reflect the power flow balance in the system, hence the converter operation can be controlled. The disadvantage of this architecture is that the system is prone to single point failure. For the PBIM system with DC couple architeture, a unidirectional boost converter is used to boost up the PV voltage and perform MPPT/curtail algorithm. A bidirectional buck-boost converter is used to boost up the battery voltage during discharging operation and step-down the DC bus voltage during charging operation. The inverter is set to have constant modulation since the DC bus voltage is already regulated.

2. **How does the control system manage the power flow in the PBIM system to perform peak shaving and off-grid self-consumption strategies?**

    - **What type of the control mechanisms are used for the converters operation, MPPT operation, and PV-curtail operation in the PBIM system?** For the MPPT algorithm, the incremental conduction method is used. For the PV-curtail algorithm, the PV operating point is shifted to the right side of the maximum power point in order to decrease the PV generation. This is done by increasing the PV voltage reference until the PV generation is lower than the load demand. Both of this algorithm will send the PV voltage reference to the unidirectional boost converter controller. A multi-loop PI control mechanism is used to control the boost converter operation. Controller has to determine the duty cycle in order to achieve the desired PV voltage reference. Next, after the power flow calculation between the PV generation and the load demand is conducted, the power deficit/surplus is reflected by the DC bus voltage. This DC bus voltage is regulated by the bidirectional buck-boost converter. A multi-loop PI control mechanism is also used to control the bidirectional buck-boost converter.

- **Which modes of operation are needed for the implementation of the chosen energy management strategies?** There are seven power flow modes in the PBIM system. For the off-grid self-consumption application, all the possible modes except mode 6 are utilized. On the other hand, modes 2 and 4 are not used in the peak shaving application, while the other modes are employed in this application.

3. **How effective is the off-grid self-consumption strategy for the PBIM application in Cambodia considering the Load of Loss Probability, PV generation reduction, and the energy exchange?** The off-grid PBIM system in Cambodia consists of one PV panel and eigth batteries in series (520 Wh). The chosen sizing resulted on the LLP of 2.60% for the whole year and less than 10% per month. During dry season, the PV generation was curtailed by 55-62% to avoid excess energy, while the PV generation was curtailed by 20% during rainy season. This PV-curtail operation eliminates the power dump problem. Regarding the energy exchange, total loss of the system is around 17%, which is caused by the converters efficiency. To conclude, the PBIM system with off-grid self-consumption strategy in Cambodia delivers good performance.

4. **How effective is the peak shaving strategy for the PBIM application in the Netherlands considering the system autarky during peak hours?** For the grid-connected PBIM in the Netherlands, one PV module with eigth batteries in series are used (520 Wh). The system drawn 555.35 kWh from the grid for the entire peak hours in one year. The monthly system autarky varies between 6-16%, where the lowest value occurs during winter, and the highest value occurs during summer. To provide better system autarky, the number of batteries per PBIM should be increased, or multiple PBIM should be installed.

7.2. Recommendations

To further improve the development of PBIM system, various recommendations regarding further research are given as follows:

- In this work, the controller for the inverter is not discussed. The detail of the inverter modulation control can be discussed further. Hence the behaviour of the AC output (i.e. voltage) can be analyzed.
- The components degradation is not taken into account in this research. The effect of component degradation can be taken into account to evaluate the system performance for a long period of operation.
- In both case studies, only one PBIM is used., hence there is no discussion regarding how to control the operation of multiple PBIMs. For further research. The development of PBIM concept needs a control strategy to operate multiple PBIMs, so it the PBIM system can be applied in a higher load (higher than household).

Bibliography

[1] B. P. Global, *Bp statistical review of world energy,* London, 67th Edition, BP Statistical (2018).

[2] J. F. Reynaud, C. Alonso, P. Aloisi, C. Cabal, B. Estibals, G. Rigobert, G. Sarre, H. Rouault, D. Mourzagh, F. Mattera, and S. Genies, *Multifunctional module lithium-ion storage and photovoltaic conversion of solar energy,* in *Conference Record of the IEEE Photovoltaic Specialists Conference* (2008).

[3] V. Vega-Garita, L. Ramirez-Elizondo, and P. Bauer, *Physical integration of a photovoltaic-battery system: A thermal analysis,* Applied Energy **208**, 446 (2017).

[4] N. A. Rahim, H. W. Ping, J. Selvaraj, *et al.*, *Photovoltaic module modeling using simulink/matlab,* Procedia Environmental Sciences **17**, 537 (2013).

[5] *Datasheet-BlueSolar-Polycrystalline-Panels-EN,* .

[6] *AMP20M1HD-A,* .

[7] R. de Ferranti, D. Fulbrook, J. McGinley, and S. Higgins, *Switching on: Cambodia's path to sustainable energy security mekong strategic partners january 2016,* Phnom Penh (2016).

[8] V. Vega-Garita, A. P. Harsarapama, L. Ramirez-Elizondo, and P. Bauer, *Physical integration of pv-battery system: Advantages, challenges, and thermal model,* in *Energy Conference (ENERGYCON), 2016 IEEE International* (IEEE, 2016) pp. 1–6.

[9] R. Fu, D. Feldman, R. Margolis, M. Woodhouse, and K. Ardani, *Us solar photovoltaic system cost benchmark: Q1 2017,* Golden: National Renewable Energy Laboratory (2017).

[10] V. Salas, *Charles iii university of madrid, madrid, spain,* The Performance of Photovoltaic (PV) Systems: Modelling, Measurement and Assessment , 251 (2016).

[11] J. Reynaud, O. Gantet, P. Aloïsi, B. Estibals, and C. Alonso, *New adaptive supervision unit to manage photovoltaic batteries,* in *Industrial Electronics, 2009. IECON'09. 35th Annual Conference of IEEE* (IEEE, 2009) pp. 664–669.

[12] J. Reynaud, O. Gantet, P. Aloisi, B. Estibals, and C. Alonso, *A novel distributed photovoltaic power architecture using advanced li-ion batteries,* in *Power Electronics and Motion Control Conference (EPE/PEMC), 2010 14th International* (IEEE, 2010) pp. S9–6.

[13] L. Barois, *The PV-Battery Integrated Module: Energy Storage Siz-ing,* .

[14] V. Vega-Garita, L. Ramirez-Elizondo, G. R. C. Mouli, and P. Bauer, *Review of residential pv-storage architectures,* in *Proc. IEEE International Energy Conference (ENERGYCON)* (2016) pp. 85–94.

[15] N. Shani, *MSc Thesis Architecture of Integrated PV-Battery Module: modeling, simulation, and comparison,* .

[16] A. Mirzaei, M. Forooghi, A. A. Ghadimi, A. H. Abolmasoumi, and M. R. Riahi, *Design and construction of a charge controller for stand-alone PV/battery hybrid system by using a new control strategy and power management,* Solar Energy **149**, 132 (2017).

[17] O. Isabella, A. Smets, K. Jäger, M. Zeman, and R. van Swaaij, *Solar energy: The physics and engineering of photovoltaic conversion, technologies and systems,* UIT Cambridge Limited (2016).

[18] E. Serban, M. Ordonez, C. Pondiche, K. Feng, M. Anun, and P. Servati, *Power Management Control Strategy in Photovoltaic and Energy Storage for Off-Grid Power Systems,* (2016).

[19] L. Olatomiwa, S. Mekhilef, M. S. Ismail, and M. Moghavvemi, *Energy management strategies in hybrid renewable energy systems: A review,* (2016).

[20] C. J. Sarasa-Maestro, R. Dufo-López, and J. L. Bernal-Agustín, *Analysis of photovoltaic self-consumption systems,* Energies (2016), 10.3390/en9090681.

[21] G. Karmiris and T. Tengnér, *Peak shaving control method for energy storage,* .

[22] O. Tremblay, L.-A. Dessaint, and A.-I. Dekkiche, *A generic battery model for the dynamic simulation of hybrid electric vehicles,* in *Vehicle Power and Propulsion Conference, 2007. VPPC 2007. IEEE* (Ieee, 2007) pp. 284–289.

[23] Y. Pragistio, *Evaluating Temperature Impact on Solar Home Systems (SHS): From the components to the systems level,* (2018).

[24] G. R. Walker, P. C. Sernia, S. Kouro, J. I. Leon, D. Vinnikov, L. G. Franquelo, Q. Li, P. Wolfs, J. M. Carrasco, L. G. Franquelo, J. T. Bialasiewicz, S. S. Member, E. Galván, R. C. P. Guisado, S. S. Member, M. Ángeles, M. Prats, J. I. León, and N. Moreno-alfonso, *Power-Electronic Systems for the Grid Integration of Renewable Energy Sources : A Survey,* IEEE Transactions on Power Electronics **53**, 1002 (2006).

[25] D. Sheet and A. Microinverters, *ABB micro inverter system MICRO-0.25/0.3/0.3HV-I-OUTD 0.25kW to 0.3kW,* .

[26] Z. Q. N. Narayan and J. P. g. J.c-c. Diehl, *Stochastic load profile construction for the multi-tier framework for household electricity access using off-grid DC appliances,* (2018).

[27] P. Highlights, *UN60EH6000,* , 8.

[28] B. Asare-Bediako, W. Kling, and P. Ribeiro, *Future residential load profiles: Scenario-based analysis of high penetration of heavy loads and distributed generation,* Energy and Buildings **75**, 228 (2014).

A

Datasheets

www.jinkosolar.com

Solar JinKO
Building Your Trust in Solar

JKM265P-60
245-265 Watt
POLY CRYSTALLINE MODULE

Positive power tolerance of 0/+3%

ISO9001:2008、ISO14001:2004、OHSAS18001 certified factory.
IEC61215、IEC61730 certified products.

KEY FEATURES

4 Busbar Solar Cell:
4 busbar solar cell adopts new technology to improve the efficiency of modules , offers a better aesthetic appearance, making it perfect for rooftop installation.

High Efficiency:
High module conversion efficiency (up to 16.19%), through innovative manufacturing technology.

Low-light Performance:
Advanced glass and solar cell surface texturing allow for excellent performance in low-light environments.

Severe Weather Resilience:
Certified to withstand: wind load (2400 Pascal) and snow load (5400 Pascal).

Durability against extreme environmental conditions:
High salt mist and ammonia resistance certified by TUV NORD.

LINEAR PERFORMANCE WARRANTY

10 Year Product Warranty • 25 Year Linear Power Warranty

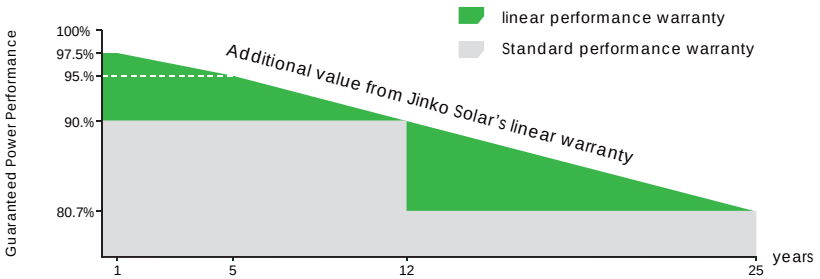

Engineering Drawings

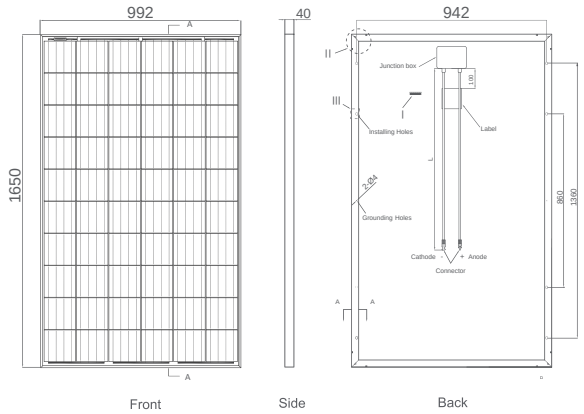

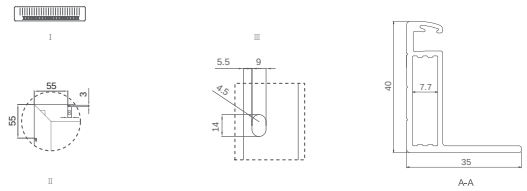

Packaging Configuration

(Two boxes=One pallet)

25pcs/ box, 50pcs/pallet, 700 pcs/40'HQ Container

Electrical Performance & Temperature Dependence

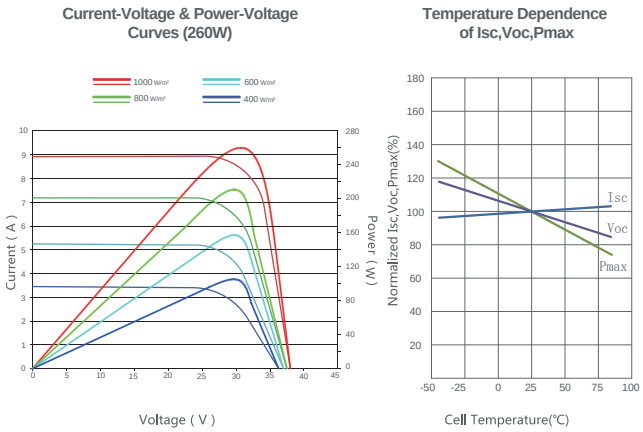

Mechanical Characteristics

Cell Type	Poly-crystalline 156×156mm (6 inch)
No.of cells	60 (6×10)
Dimensions	1650×992×40mm (65.00×39.05×1.57 inch)
Weight	19.0 kg (41.9 lbs)
Front Glass	3.2mm, High Transmission, Low Iron, Tempered Glass
Frame	Anodized Aluminium Alloy
Junction Box	IP67 Rated
Output Cables	TÜV 1×4.0mm^2, Length: 900mm or Customized Length

SPECIFICATIONS

Module Type	JKM245P		JKM250P		JKM255P		JKM260P		JKM265P	
	STC	NOCT	STC	NOCT	STC	NOCT	STC	NOCT	STC	NOCT
Maximum Power (Pmax)	245Wp	181Wp	250Wp	184Wp	255Wp	189 Wp	260Wp	193Wp	265Wp	197Wp
Maximum Power Voltage (Vmp)	30.1V	27.8V	30.5V	28.0V	30.8V	28.5V	31.1V	28.7V	31.4V	29.0V
Maximum Power Current (Imp)	8.14A	6.50A	8.20A	6.56A	8.28A	6.63A	8.37A	6.71A	8.44A	6.78A
Open-circuit Voltage (Voc)	37.5V	34.8V	37.7V	34.9V	38.0V	35.2V	38.1V	35.2V	38.6V	35.3V
Short-circuit Current (Isc)	8.76A	7.16A	8.85A	7.21A	8.92A	7.26A	8.98A	7.31A	9.03A	7.36A
Module Efficiency STC (%)	14.97%		15.27%		15.58%		15.89%		16.19%	
Operating Temperature(℃)	-40℃~+85℃									
Maximum system voltage	1000VDC (IEC)									
Maximum series fuse rating	15A									
Power tolerance	0~+3%									
Temperature coefficients of Pmax	-0.41%/℃									
Temperature coefficients of Voc	-0.31%/℃									
Temperature coefficients of Isc	0.06%/℃									
Nominal operating cell temperature (NOCT)	45±2℃									

STC: Irradiance 1000W/m^2 Cell Temperature 25°C AM=1.5

NOCT: Irradiance 800W/m^2 Ambient Temperature 20°C AM=1.5 Wind Speed 1m/s

* Power measurement tolerance: ± 3%

Nanophosphate® Lithium Ion Prismatic Pouch Cell

AMP20*m1*HD-A

KEY FEATURES AND BENEFITS

- High usable energy over a wide state of charge (SOC) range and very low cost per Watt-hour
- Excellent abuse tolerance and superior cycle life from A123's patented Nanophosphate® lithium ion chemistry
- High power with over 2,400 W/kg and 4,500 W/L

AMP20 Cell Specifications	
Cell Dimensions (mm)	7.25 x 160 x 227
Cell Weight (g)	496
Cell Capacity (minimum, Ah)	19.6
Energy Content (nominal, Wh)	65
Discharge Power (nominal, W)	1200
Voltage (nominal, V)	3.3
Specific Power (nominal, W/kg)	2400
Specific Energy (nominal, Wh/kg)	131
Energy Density (nominal, Wh/L)	247
Operating Temperature	-30°C to 55°C
Storage Temperature	-40°C to 60°C

Abuse Test	Test Result
Nail Penetration	Pass – EUCAR 3
Overcharge	Pass – EUCAR 3
Over-discharge	Pass – EUCAR 3
Thermal Stability	Pass – EUCAR 4
External Short	Pass – EUCAR 3
Crush	Pass – EUCAR 3

APPLICATIONS

PHEV and EV Passenger Vehicles

PHEV and EV Commercial Vehicles

Utility-scale Storage

A123 SYSTEMS

www.a123systems.com

MD100105-02

Nanophosphate® Lithium Ion Prismatic Pouch Cell

AMP20*m1*HD-A

POWER

10s Pulse Power Capability vs State of Charge at 23°C, Using FreedomCAR HPPC

Vmax = 3.8 V, Vmin = 1.6 V

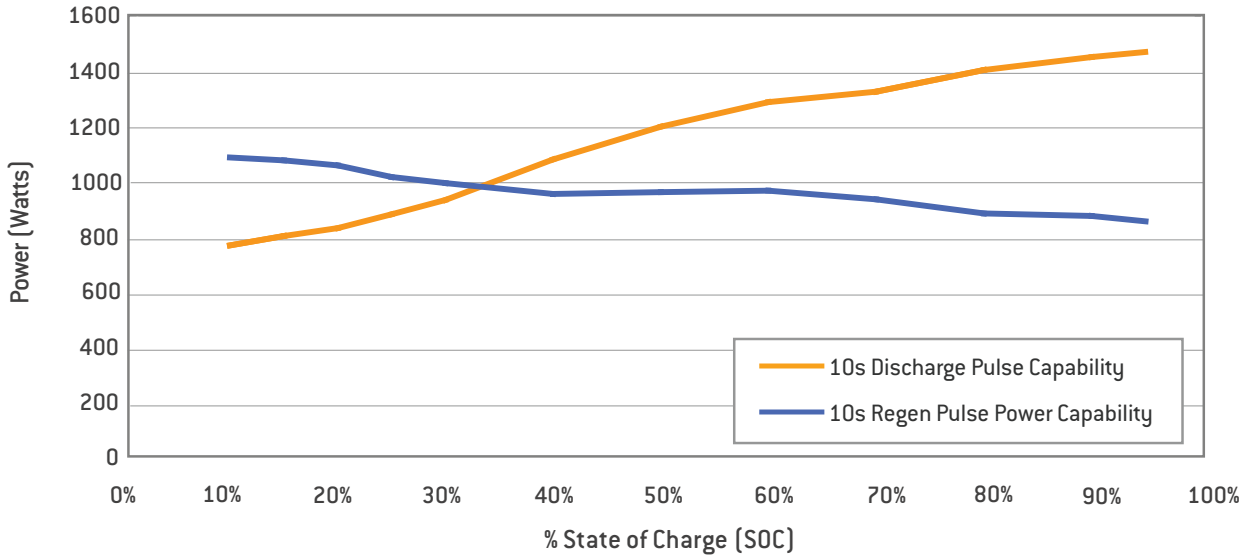

CYCLE LIFE

Capacity vs Cycles

100% Depth of Discharge (DOD), +1C/-2C, 23°C

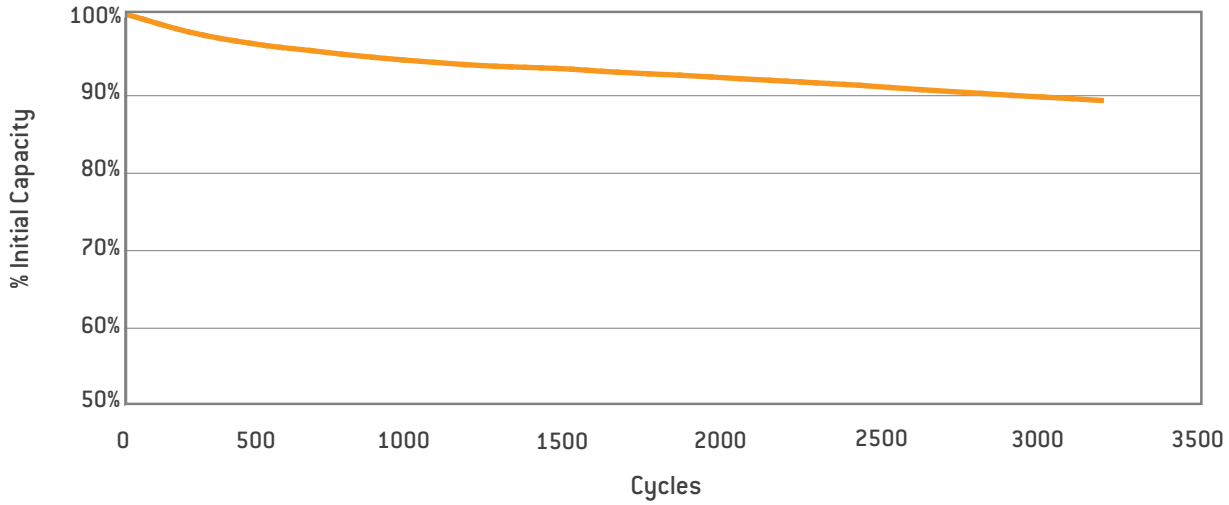

Preliminary specifications, performance may vary depending on use conditions and application.

A123 Systems makes no warranty explicit or implied with this datasheet. Contents subject to change without notice.

CORPORATE HEADQUARTERS

A123 Systems, Inc.

200 West Street

Waltham, MA 02451

(617) 778-5700

www.a123systems.com

MD100105-02

PRODUCT HIGHLIGHTS

LED TV

- Full HD 1080p
- LED picture quality
- Clear Motion Rate 240

Enjoy a cinema-like experience in the comfort of your own home.

This LED HDTV allows you to immerse yourself in a Full High-Definition 1080p viewing experience. ConnectShare™ Movie lets you watch videos, play music or view photos from a USB drive. Simply plug it into the TV's USB port and enjoy content on the big screen with friends and family. And use the two HDMI® ports to easily connect multiple compatible AV devices at the same time. The impressive picture quality, excellent sound technology and slim profile design will transform how you watch TV.

UN60EH6000

60" Class (60.0" Diagonal) LED HDTV with 1080p Resolution

PICTURE QUALITY

- Full HD 1080p
- Clear Motion Rate 240
- Wide Color Enhancer Plus

AUDIO

- 10W x 2
- Dolby® Digital Plus/Dolby® Pulse
- SRS TheaterSound HD™

CONNECTIONS

- HDMI®: 2
- USB: 1
- Component in: 1
- Digital audio output: 1 optical
- ConnectShare™ Movie

NET DIMENSIONS (WxHxD)

TV without stand: 54.1" x 31.8" x 3.7"
TV with stand: 54.1" x 33.8" x 13.0"

UPC

036725236691

LED TV SERIES 6

UN60EH6000 60" Class (60.0" Diagonal) LED HDTV with 1080p Resolution

PICTURE QUALITY

Full HD 1080p: With twice the resolution of standard HD TVs, Samsung TVs deliver images that are guaranteed to amaze and bring pleasure to your home entertainment experience. The realistic texture of Full HD images invites you to enjoy a viewing experience that redefines reality.

Clear Motion Rate (CMR): A comprehensive measure of a TV's ability to display images in motion. The higher the CMR, the better. Samsung achieves high CMR numbers based on panel processing advancements. See the picture quality difference for yourself.

Wide Color Enhancer Plus: Allows you to see picture color the way the director originally intended, brought to life on your screen to bring you exceptionally vibrant, yet natural-looking images and depicts subtle details and tones.

AUDIO

10 watts x 2 audio power stereo broadcast reception: Supports multi-channel sound (MTS) and second audio program (SAP) with 181-channel capacity.

Dolby® Digital Plus/ Dolby® Pulse: An advanced surround sound audio processing feature designed to optimize the TV's sound quality when viewing and listening to Internet movies, Internet music and other content played back from wired or wireless mobile phones, PCs and tablet devices.

SRS TheaterSound HD™: A high-definition audio experience that delivers surround sound multi-channel content, using built-in TV speakers to significantly enhance both the depth and dimension of audio right through the TV. Enjoy a simulated surround sound experience!

CONNECTIONS

HDMI®: 2
HDMI® (High-Definition Multimedia Interface) is a convenient, high-quality single cable digital audio/video interface for connecting the TV to a digital cable box, satellite box, DVD/Blu-ray Disc® Player, PC computers, PC portable devices, new generation tablets and devices featuring the HDMI® output.

USB: 1
Universal Serial Bus (USB) is an industry standard for connecting a variety of computer, audio and video devices to the TV. USB movie capability allows the streaming of video from storage devices, cameras, camcorders and USB drives.

Component in: 1

Digital audio output: 1 optical

ConnectShare™ Movie: Have movies and pictures on a USB drive? Now easily view that content right on the TV. Just plug the drive into the USB port and you are ready for a big screen experience.

NET DIMENSIONS & WEIGHT (WxHxD)

TV without stand: 54.1" x 31.8" x 3.7"
TV without stand weight: 54.7 lbs
TV with stand: 54.1" x 33.8" x 13.0"
TV with stand weight: 60.4 lbs

SHIPPING DIMENSIONS & WEIGHT (WxHxD)

Dimensions: 66.2" x 36.8" x 7.9"
Weight: 74.5 lbs

WARRANTY

1-year parts and 1-year labor warranty (90-days parts and labor for commercial use) with in-home service, backed by Samsung toll-free support.

ORDER CODE

UN60EH6000FXZA

UPC

036725236691

SAMSUNG